Journal of Colloid and Interface Science 494 (2017) 223–241

Contents lists available at ScienceDirect

Journal of Colloid and Interface Science

journal homepage: www.elsevier.com/locate/jcis

Regular Article

Optimization of cellulose and sugarcane bagasse oxidation: Application for adsorptive removal of crystal violet and auramine-O from aqueous solution

Luide Rodrigo Martins, Josilene Aparecida Vieira Rodrigues, Oscar Fernando Herrera Adarme, Tânia Márcia Sacramento Melo, Leandro Vinícius Alves Gurgel, Laurent Frédéric Gil *

Departamento de Química, Instituto de Ciências Exatas e Biológicas, Universidade Federal de Ouro Preto, Campus Universitário Morro do Cruzeiro, s/n°, Bauxita, 35400-000 Ouro Preto, Minas Gerais, Brazil

GRAPHICAL ABSTRACT

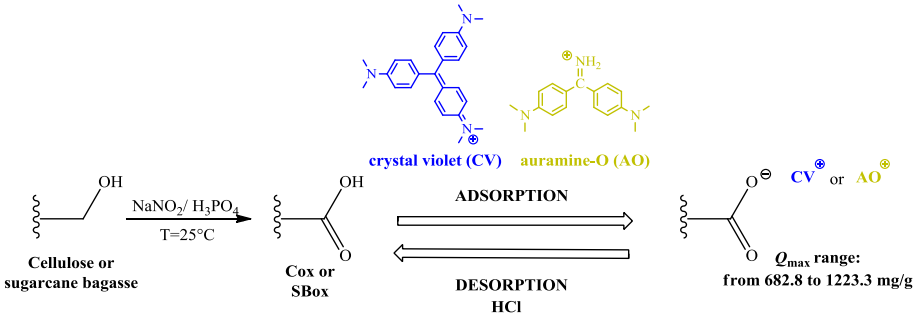

ARTICLE INFO

Article history:
Received 26 October 2016
Revised 19 January 2017
Accepted 22 January 2017
Available online 25 January 2017

Keywords:
Oxidized cellulose
Oxidized sugarcane bagasse
Adsorption
Desorption
Crystal violet
Auramine-O

ABSTRACT

Cellulose (Cel) and sugarcane bagasse (SB) were oxidized with an H_3PO_4-$NaNO_2$ mixture to obtain adsorbent materials with high contents of carboxylic groups. The oxidation reactions of Cel and SB were optimized using design of experiments (DOE) and response surface methodology (RSM). The optimized synthesis conditions yielded Cox and SBox with 4.8 mmol/g and 4.5 mmol/g of carboxylic acid groups, respectively. Cox and SBox were characterized by FTIR, TGA, PZC and solid-state ^{13}C NMR. The adsorption of the model cationic dyes crystal violet (CV) and auramine-O (AO) on Cox and SBox in aqueous solution was investigated as a function of the solution pH, the contact time and the initial dye concentration. The adsorption of CV and AO on Cox was described by the Elovich equation and the pseudo-first-order kinetic model respectively, while the adsorption of CV and AO on SBox was described by the pseudo-second-order kinetic model. Adsorption isotherms were well fitted by the Langmuir and Konda models, with maximum adsorption capacities (Q_{max}) of 1117.8 mg/g of CV and 1223.3 mg/g of AO on Cox and 1018.2 mg/g of CV and 682.8 mg/g of AO on SBox. Desorption efficiencies were in the range of 50–52% and re-adsorption capacities varied from 65 to 81%, showing the possibility of reuse of both adsorbent materials.

1. Introduction

Highly colored effluents, especially from textile industries, have been a matter of great environmental interest [1]. Dyes are chem-

* Corresponding author.
E-mail address: laurent@iceb.ufop.br (L.F. Gil).

http://dx.doi.org/10.1016/j.jcis.2017.01.085
0021-9797/

ical compounds that can bind to surfaces or tissues to add color. Most dyes are complex organic molecules, which must be resistant in various situations, such as the presence of detergents, sunlight and heat. Every year, about 700,000 tons of dyes are produced and about 100,000 tons are commercially available.

The applications of dyes are diverse and some industries such as cosmetics, leather tanning, food, paper, plastics production, printing rubber and textile demand a large amount of synthetic dyes [2]. Realistic data on the amount of dyes dumped into the environment are not available at present time. However, it is estimated that about 1–2% is lost in dye production and 1–10% during use. Due to their large-scale production and extensive applications, synthetic dyes can thus cause environmental pollution and present serious health risks [3]. These compounds can cause unwanted changes in the color of water bodies and affect the photosynthesis of algae. In addition, some dyes and their byproducts are toxic to aquatic life and mutagenic and/or carcinogenic to humans [4].

Several methods have been developed for the removal of dyes from wastewaters. These methods can include processes such as adsorption, advanced oxidation processes (POAs), anaerobic digestion (AD), coagulation and flotation, gravity separation, enzymatic decomposition, photocatalysis and ultrafiltration. However, among these various available treatment techniques, adsorption is advantageous because of its high efficiency, ease of operation, good benefit/cost ratio, the availability of different adsorbent types and the possibility of reusing the adsorbent and/or adsorbate [5,6].

An effective adsorbent must consist of an aqueous-insoluble matrix that has good mechanical, chemical and thermal stability. Furthermore, it needs to have active groups on its surface that allow interactions with the pollutants that are to be removed [7]. Agricultural wastes such as sugarcane bagasse (SB) are very attractive renewable resources due to their low cost and easy availability and they represent excellent supports for new bioadsorbents [8,9]. Brazil is the world's leading producer of sugarcane. According to the last official survey from the National Company of Supply (CONAB), an agency of the Brazilian Ministry of Agriculture, the production of sugarcane in the 2015/2016 season was estimated to be about 658.7 million tons [10]. Since sugarcane bagasse is an important by-product of brazilian agroindustry, there is great interest in reusing it to produce new materials with valuable applications.

Sugarcane bagasse is mainly composed of 40–50% cellulose, 25–30% hemicelluloses and 20–25% lignin [11]. Cellulose, the most abundant and renewable biopolymer in nature, consists of a linear homopolymer of β(1 → 4) linked β-D-anhydroglucopyranose units (AGU). Its molecular structure presents many possibilities for chemical modification reactions due to the reactivity of the hydroxyl groups present in AGU [12]. At the present moment, there are several studies in the literature that have used sugarcane bagasse and cellulose as adsorbents for various types of pollutants [13,14]. In general, the solid supports are chemically modified to increase their affinity for the adsorbates that are to be removed, thereby increasing their adsorption capacity and selectivity [15–19]. The main modifications of hydroxyl groups that have been performed are esterification [20], etherification [21] and halogenation [22]. An interesting way to chemically modify cellulose or lignocellulose biomass is through the oxidation of hydroxyl groups. Depending on the oxidizing agent used, different kinds of changes in the structure and crystallinity of the lignocellulose biomass can be obtained, resulting in different types of modifications in the physical and chemical properties of the oxidized products [23]. For example, reaction of cellulose with sodium periodate selectively oxidizes the hydroxyl groups at carbons 2 and 3 of AGU to produce a C—C cleavage and a dialdehyde functionality [24]. When the TEMPO-hypochlorite/bromide [25], H_3PO_4/HNO_3-$NaNO_2$ [26], H_3PO_4-$NaNO_3$/$NaNO_2$ [27] or H_3PO_4-$NaNO_2$ systems [28] are used as oxidants, the oxidation of cellulose will occur preferentially at carbon 6 of AGU, allowing the introduction of carboxylic acid groups into the structure of the biopolymer. Such chemical modifications can provide materials with new and interesting properties for various applications [29].

This study aimed to evaluate the modification of cellulose and sugarcane bagasse by oxidation with an H_3PO_4-$NaNO_2$ mixture. Initially, the first part of our investigations focused on the oxidation of cellulose. Although oxidation of cellulose has already been studied before [25–28], this is the first study describing optimization by design of experiments of the oxidation of cellulose using H_3PO_4-$NaNO_2$ system. The second part of this study describes for the first time the oxidation of sugarcane bagasse using H_3PO_4-$NaNO_2$ system and its use for adsorptive removal of cationic dyes from aqueous solution. The oxidation reactions were optimized using a design of experiments (DOE) and a response surface methodology (RSM). The variables chosen for optimization were the amounts of H_3PO_4 and $NaNO_2$ and the reaction time. The main response evaluated was the number of carboxylic acid groups introduced into cellulose and sugarcane bagasse. After optimizing the oxidation process, the materials produced, named oxidized cellulose (Cox) and oxidized sugarcane bagasse (SBox), were used for the removal of the model cationic dyes crystal violet (CV) and auramine-O (AO) from aqueous solution. The adsorption studies were assessed as a function of the contact time (kinetics), the solution pH and the initial dye concentration.

2. Material and methods

2.1. Material

Grade 3MM Chr cellulose chromatography paper (Cat. No. 3030-861) was purchased from the Whatman Company, Maidstone, England. The cationic dyes auramine-O (C.I.: 41,000, $C_{17}H_{21}N_3$·HCl, λ_{max} = 432 nm and MW = 303.83 g/mol) and crystal violet (C.I.: 42,555, $C_{25}H_{30}N_3Cl$, λ_{max} = 584 nm and MW = 407.98 g/mol) (see Fig. 1) were purchased from Vetec (Brazil) and used without further purification. Phosphoric acid (85%) was purchased from Neon (Brazil). Sodium nitrite and sodium hydroxide were purchased from Synth (Brazil).

2.2. Sugarcane bagasse and cellulose preparation

Sugarcane bagasse (SB) was collected from an industrial alcohol producing plant at Ouro Preto, Minas Gerais, Brazil. SB was prepared for the oxidation reactions according to the procedure described by Ramos et al. [30]. Sheets of Whatman cellulose paper (Cel) were cut into 50 mm^2 pieces and milled in an analytical mill (IKA, model A11 basic).

2.3. Statistical design of experiments

The oxidation reaction of Cel and SB was optimized using a 2^3 central composite design (CCD). The independent variables evaluated were the volume of H_3PO_4 (mL), the weight of $NaNO_2$ (mg) and the reaction time (h). The dependent variable evaluated was the amount of carboxylic acid groups (n_{COOH}) introduced into Cox and SBox. The experiments were performed using two orthogonal blocks that satisfied the rotatability condition. Therefore, the effects of these blocks did not affect the estimated parameters in the response surface model. The first block (experiments 1–11) was a 2^3 experimental design with triplicates at the central point (screening experiments) and the second block was made by the addition of axial points in the levels of the experimental design (experiments 12–17) [31]. The full design matrix of the experi-

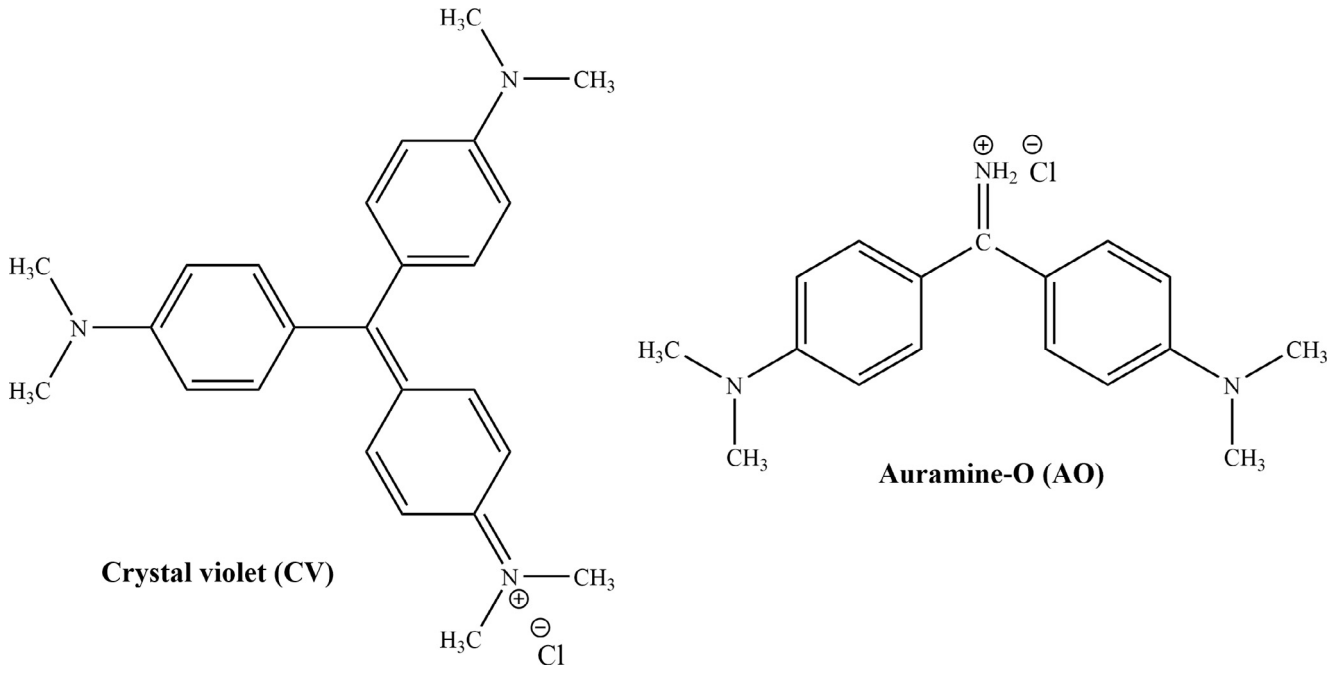

Fig. 1. Chemical structures of crystal violet (CV) and auramine-O (AO).

ments (1–17) for the 2^3 central composite design for Cel and SB oxidation is shown in Table 1.

Statistical analyses were carried out with a significance level of 95%. Pure error was chosen to evaluate the experimental error. The relevance of the linear terms and their interactions for the three independent variables was evaluated as well as their lack of fit.

The regression model in terms of the uncoded variable levels (−1, 0, +1 and ±1.682) is a polynomial equation of second degree in terms of the dependent variable (*DV*), as shown in Eq. (1):

$$DV = a_0 + a_1 t + a_2 V_{H_3PO_4} + a_3 w_{NaNO_2} + a_4 t^2 + a_5 V_{H_3PO_4}^2 + a_6 w_{NaNO_2}^2 + a_7 t V_{H_3PO_4} + a_8 t w_{NaNO_2} + a_9 V_{H_3PO_4} w_{NaNO_2} \quad (1)$$

where *DV* is the dependent variable, $a_0, a_1, a_2, a_3, a_4, a_5, a_6, a_7, a_8$ and a_9 are the regression coefficients obtained by fitting the experimental data to the model, t is the reaction time (h), $V_{H_3PO_4}$ (mL) is the volume of phosphoric acid and w_{NaNO_2} (mg) is the weight of sodium nitrite.

2.4. Oxidation of cellulose and sugarcane bagasse

The oxidation reactions of Cel and SB were performed in 250 mL Erlenmeyer flasks at 25 °C. In a typical procedure, 1.000 g of Cel or SB was placed into the flasks and H_3PO_4 was added under agitation. Afterwards, $NaNO_2$ was added to the flasks, with vigorous agitation for approximately 10 min. After addition of $NaNO_2$, the suspension was left to stand for a set time. The oxidized material (Cox or SBox) was separated from the oxidation mixture by vacuum filtration in a sintered Büchner glass funnel (porosity 2) and washed with distilled water until the pH was ~7. The oxidized material was dried at 65 °C in an oven for 4 h. The volumes of H_3PO_4, weights of $NaNO_2$ and reaction times used in each oxidation experiment are shown in Table 1.

The experimental conditions used to prepare the materials for the adsorption experiments were 5.000 g of Cel or SB, 80.0 mL of H_3PO_4, 4.000 g of $NaNO_2$ and a reaction time of 5 h.

Table 1
The design matrix of experiments for the 2^3 central composite design for the oxidation of cellulose and sugarcane bagasse (uncoded variable values in parentheses).

Experiment[a]	Time (h)	Volume of H_3PO_4 (mL)	Weight of $NaNO_2$ (mg)	n_{COOH} Cel (mmol/g)	n_{COOH} SBox (mmol/g)
1	−1 (3)	−1 (6.0)	−1 (300.0)	2.546	2.536
2	1 (7)	−1 (6.0)	−1 (300.0)	3.425	2.680
3	−1 (3)	1 (16.0)	−1 (300.0)	2.373	2.307
4	1 (7)	1 (6.0)	−1 (300.0)	4.224	2.605
5	−1 (3)	−1 (6.0)	1 (800.0)	2.543	2.536
6	1 (7)	−1 (6.0)	1 (800.0)	3.521	2.780
7	−1 (3)	1 (16.0)	1 (800.0)	3.800	3.311
8	1 (7)	1 (16.0)	1 (800.0)	4.998	3.630
9	0 (5)	0 (11.0)	0 (550.0)	4.801	3.491
10	0 (5)	0 (11.0)	0 (550.0)	4.516	3.302
11	0 (5)	0 (11.0)	0 (550.0)	4.824	3.302
12	−1.682 (1.6)	0 (11.0)	0 (550.0)	5.793	5.791
13	1.682 (8.4)	0 (11.0)	0 (550.0)	7.043	6.285
14	0 (5)	−1.682 (2.6)	0 (550.0)	5.193	5.177
15	0 (5)	1.682 (19.4)	0 (550.0)	6.618	6.702
16	0 (5)	0 (11.0)	−1.682 (129.6)	5.730	4.780
17	0 (5)	0 (11.0)	1.682 (970.5)	7.398	6.384

[a] Weight of Cel and SB was fixed at 1.000 g for all oxidation experiments.

2.5. Characterization of Cox and SBox

2.5.1. Amount of carboxylic acid groups (n_{COOH})

The amount of carboxylic acid groups on Cox and SBox was determined by acid-base back-titration. In a typical procedure, 0.0500 g of Cox or SBox was added to a 250 mL Erlenmeyer flask together with 100.0 mL of an aqueous NaOH standard solution (0.01 mol/L). The flasks were stirred at 100 rpm for 1 h. The suspensions were separated by a single filtration and three aliquots of 25.0 mL of each filtrate were titrated with an aqueous HCl standard solution (0.01 mol/L) [8,11]. The n_{COOH} was calculated using Eq. (2):

$$n_{COOH}/(\text{mmol/g}) = \frac{[C_{NaOH}V_{NaOH} - 4(C_{HCl}V_{HCl})]}{w} \times 100 \quad (2)$$

where C_{NaOH} is the concentration of aqueous NaOH standard solution (mmol/L), C_{HCl} is the concentration of aqueous HCl standard solution (mmol/L), V_{NaOH} is the volume of NaOH solution (L), V_{HCl} is the volume of HCl spent in the titration of excessive non-reacted base (L) and w is the weight of oxidized material (Cox or SBox) (g).

2.5.2. Fourier transform infrared spectroscopy (FTIR) analysis

Samples for analyses were prepared by mixing 1 mg of Cox or SBox (dried powder) with 100 mg of spectroscopy grade KBr. The mixtures were pressed in a hydraulic press (Pike CrushIR, model 181-1110, Pike Technologies, Canada) to obtain 13 mm diameter KBr pellets. The FTIR spectra were recorded on an FTIR spectrometer (ABB Bomen, model MB 3000) with the detector set at a resolution of 4 cm^{-1}, scanning from 500 to 4000 cm^{-1}, with 32 scans per sample.

2.5.3. Solid state ^{13}C NMR analysis

The solid-state ^{13}C NMR spectrum of Cox was obtained on a Bruker DRX-500 spectrometer at a frequency of 125.72 MHz with an accumulation of 4096 scans.

2.5.4. Point of zero charge (PZC)

The point of zero charge (PZC) of Cox and SBox was determined using the mass titration method as described by Noh and Schwarz [32]. Three aqueous 0.01 mol/L $NaNO_3$ solutions with pH values of 3, 6 and 11 were prepared adjusting the pH of the solutions with aqueous 0.1 mol/L HNO_3 and 0.1 mol/L NaOH. Five aliquots of 20.0 mL were taken from the solutions of different pH and transferred to 125 mL Erlenmeyer flasks. Different amounts of the oxidized materials were then added to the flasks to give suspensions of 5%, 10%, 15%, 20% and 25% (w/v). The equilibrium pH values were measured after 24 h of agitation at 25 °C and 130 rpm using a pH meter (Hanna Instruments, model HI 223). The PZC was calculated at the convergence point of the three curves of equilibrium pH against the weight-to-volume percentage of the oxidized material.

2.5.5. Thermogravimetric analysis (TGA)

Thermogravimetric analysis was carried out in a Shimadzu DTG-60H simultaneous TG-DTA. Samples of 2.5 mg of Cox and SBox (powder) were placed on aluminum pans. TGA experiments were carried out under an N_2 atmosphere at a flow rate of 100 mL/min. Samples were heated from 25 to 800 °C at a linear heating rate of 20 °C/min.

2.6. Scanning electron microscopy (SEM)

The morphological features of Cel and Cox and SB and SBox were examined with a Vega3 SB scanning electron microscope (Tescan/Oxford Instruments), using a tungsten filament voltage of 20 keV. Dried powder samples were dispersed on a graphite ribbon fixed on aluminum sample holders and sputter-coated with gold in a modular high-vacuum coating system (Quorum Technologies, model Q150R ES).

2.7. Adsorption experiments

Adsorption experiments were undertaken to determine the effect of solution pH, contact time and initial dye concentration on the adsorption of CV and AO on Cox and SBox. All adsorption experiments were performed in duplicate using the following typical procedure. Samples of 20.0 mg of Cox or SBox were weighed into 250 mL Erlenmeyer flasks and 100.0 mL of dye solution of known concentration at a set pH was added. The flasks were placed at 25 °C in a shaker incubator (Tecnal, model TE-424) and stirred at 150 rpm for a set time. Then, the suspensions were centrifuged (Excelsa II mod. 206 BL) at 3600 rpm for 20 min and the supernatant was taken to determine the concentration of CV or AO. The concentration of the dye in the supernatant was determined measuring the absorbance on a UV–Vis spectrophotometer (BIOSPECTRO, SP220) at wavelengths of maximum absorption of 584 nm for CV and 432 nm for AO. The dye concentration was calculated from an analytical curve of absorbance against dye concentration. The adsorption capacity, q, was calculated using Eq. (3):

$$q/(\text{mg/g}) = \frac{(C_i - C_e)V}{w} \quad (3)$$

where q (mg/g) is the amount of dye adsorbed (mg) per weight of Cox or SBox (g), V (L) is the volume of dye solution, C_i (mg/L) is the initial dye concentration, C_e (mg/L) is the dye concentration at equilibrium or at time t and w (g) is the weight of Cox or SBox.

2.7.1. Effect of the solution pH on dye uptake by Cox and SBox

The effect of the solution pH on the removal of CV and AO by Cox or SBox was evaluated using an initial dye concentration of 200 mg/L and an equilibrium contact time of 12 h. The pH range studied was from 3.0 to 8.0 for both dyes.

2.7.2. Effect of contact time (kinetics) on dye uptake by Cox and SBox

The effect of contact time on the removal of CV and AO by Cox or SBox was evaluated using an initial dye concentration of 200 mg/L and a solution pH of 8. The time interval investigated was from 15 to 1440 min for both dyes.

2.7.3. Effect of initial dye concentration on dye uptake by Cox and SBox

The effect of initial dye concentration on dye uptake by Cox and SBox was examined by varying the initial dye concentration to obtain adsorption isotherms. The experiments were performed at pH 8.0 with an equilibrium time of 12 h for CV and 9 h for AO. The initial dye concentration interval was from 50 to 600 mg/L for both dyes.

2.8. Desorption and reuse of Cox and SBox

To evaluate the possibility of reuse of the adsorbent materials, desorption experiments were performed. The loading of Cox and SBox with CV and AO was performed at pH 8 with a contact time of 12 h for both dyes. Samples of 0.050 g of Cox or SBox were loaded with 100.0 mL of 500 mg/L CV or 400 mg/L AO. Further procedures were the same as described in Section 2.7. Each material was recovered by a single filtration and washed with an excess of distilled water to remove non-adsorbed dye. After drying in an oven at 60 °C for 6 h, 0.040 g of Cox-CV, Cox-AO, SBox-CV or SBox-AO were weighed into 250 mL Erlenmeyer flasks containing 100.0 mL of desorption solution. The desorption solution consisted of aqueous HCl solutions at two different concentrations,

0.05 mol/L for CV desorption and 0.01 mol/L for AO desorption. Desorption experiments were carried out at 25 °C in a shaker incubator (Tecnal, model TE-424) with an agitation speed of 150 rpm. The desorption time for Cox-CV and SBox-CV was 4 h, and 2 h for Cox-AO and SBox-AO. The concentration of dye in the desorption solutions was measured as described in Section 2.7. The desorption efficiency was calculated using Eq. (4) [33]:

$$E_{des}/\% = \left(\frac{C_e V}{Q_{T,max} w'}\right) \times 100 \quad (4)$$

where E_{des} (%) is the desorption efficiency, C_e (mg/L) is the equilibrium dye concentration in aqueous HCl desorption solution, V (L) is the volume of desorption solution, $Q_{T,max}$ (mg/g) is the maximum adsorption capacity determined by loading Cox and SBox with dyes before the desorption study and w' (g) is the weight of Cox or SBox contained in each adsorbent loaded with CV or AO (w_{dye}) used in the desorption study.

The weight of Cox and SBox contained in w_{dye} is calculated using Eq. (5):

$$w'/g = \frac{w_{dye} w}{\left(\frac{Q_{T,max} w}{1000}\right) + w} \quad (5)$$

Rearranging and simplifying Eq. (5) yields Eq. (6) as follows:

$$w'/g = \frac{w_{dye}}{\left(\frac{Q_{T,max}}{1000} + 1\right)} \quad (6)$$

where w_{dye} (g) is the weight of Cox or SBox loaded with CV or AO.

For the reuse studies, the experimental adsorption procedures were the same as previously described. The weight of adsorbent used after the desorption process was 0.020 g. The re-adsorption efficiency was calculated using Eq. (7):

$$RE/\% = \left(\frac{Q_{RE,max}}{Q_{T,max}}\right) \times 100 \quad (7)$$

where RE (%) is the re-adsorption efficiency and $Q_{RE,max}$ (mg/g) is the maximum adsorption capacity recalculated in the re-adsorption study. The value of $Q_{RE,max}$ is calculated using Eq. (8):

$$Q_{RE,max}/(mg/g) = \frac{w_D + w_{DR}}{w} \quad (8)$$

where w_D (mg) is the weight of dye desorbed from the Cox or SBox after the desorption study and w_{DR} (mg) is the weight of dye adsorbed on Cox or SBox in the re-adsorption study. The values of w_D and w_{DR} are calculated using Eqs. (9) and (10):

$$w_D/mg = \left[(w_{dye} - w')(1 - E_{des}/100)\right] \times 1000 \quad (9)$$

$$w_{DR}/mg = (C_i - C_e)V \quad (10)$$

3. Results and discussion

3.1. Optimization of cellulose and sugarcane bagasse oxidation

The optimization of the oxidation reaction of Cel and SB was carried out by measuring the dependent variable n_{COOH}, which is the most important parameter affecting the adsorption capacity of carboxylated materials. The statistically significant effects of the independent variables (volume of H_3PO_4, weight of $NaNO_2$ and reaction time) in the oxidation reaction of Cel and SB can be seen in the Pareto's chart that is shown in Fig. 2a and b.

The Pareto's chart for Cel oxidation (Fig. 2a) shows that the independent variables reaction time (10.1), volume of H_3PO_4 (6.92) and weight of $NaNO_2$ (4.72) as well as the interaction between the volume of H_3PO_4 and the weight of $NaNO_2$ (4.34) had a significant positive effect on the dependent variable n_{COOH}. It should be noted that the standardized value of the reaction time was the most significant compared with the other significant variables. The Pareto's chart for SB oxidation (Fig. 2b) shows that the weight of $NaNO_2$ (6.98) and the interaction between the volume of H_3PO_4 and the weight of $NaNO_2$ (6.25) had significant positive effects on the dependent variable n_{COOH}. The volume of H_3PO_4 was not significant (4.28), but was within the limit of the significant standardized effect (4.303). In contrast with Cel oxidation, the reaction time was not significant in SB oxidation.

For Cel oxidation, the reaction time had the most significant effect on n_{COOH}. Similar results were reported by Kumar and Yang [26] for the oxidation of cellulose using H_3PO_4/HNO_3-$NaNO_2$. According to Laisha and Sharkov [34], the dependence of the degree of oxidation on the reaction time can be explained by the accessibility of the oxidant agent to the active sites and the heterogeneity of the reaction system. For heterogeneous reactions, accessibility is a crucial factor and the reactivity of the active sites on cellulose are clearly controlled by the hydrogen bond breaking step, which also affects the degree of crystallinity of the cellulose [12,34].

Once HNO_2 is formed from the reaction between $NaNO_2$ and H_3PO_4, it can be easily converted into N_2O_3 and then into NO_2 and NO·. The latter is an odd-electron specie, which is responsible for hydrogen abstraction of cellulose, and therefore, for the attack to oxidized intermediates that produce Cel-COOH [26]. Another important element for the introduction of carboxylic functions into the Cel and SB structures is the high surface area within the foam that is formed by the production of N_2O_3 *in situ* due to the reaction between H_3PO_4 and $NaNO_2$. This phenomenon is considered to be decisive for the AGU oxidation. The excess pressure inside the bubbles also appears to be a decisive component for the oxidation process [35]. Thus, the interaction between the variables volume of H_3PO_4 and weight of $NaNO_2$ has a fundamental role in the formation of carboxylic acids, as evidenced in the Pareto's chart for Cel and SB oxidation (Fig. 2a and b).

In SB oxidation, the oxidation extent, as measured by n_{COOH}, was favored by greater quantities of the oxidizing agent $NaNO_2$. More $NaNO_2$ is probably required to oxidize sugarcane bagasse cellulose because the hemicellulose and lignin content of SB can also react with $NaNO_2$ [12].

Some studies [28,34,36,37] have suggested that H_3PO_4 also acts in the acid hydrolysis of hemicelluloses and to a smaller degree in the acid hydrolysis of lignin and cellulose. Increases in the H_3PO_4-to-solid ratio may result in an increase in the oxidation of secondary hydroxyl groups in the cellulose structure, allowing the formation of ketones and the hydrolysis of cellulose chains. Due to the reactivity of H_3PO_4 with hemicelluloses and lignin, the contribution of H_3PO_4 in the oxidation reaction of SB was less significant.

Table 2 shows the p-values and regression coefficients in terms of uncoded variables for the oxidation of Cel and SB. The quadratic polynomial equations found from modeling the experimental data showed correlation coefficients (R^2) of 0.9883 for Cel and 0.9881 for SB. Thus, in the range of independent variables studied, such equations are able to accurately predict 98.83% and 98.81% of the variation in the responses for the oxidation reactions of Cel and SB, respectively. The response surface models were evaluated using ANOVA. As can be seen in Table 3, lack of fit was not significant.

Fig. 3a–d shows the response surfaces and contour lines generated from equations obtained by modeling the experimental data for Cel and SB oxidation. It can be seen that with the reaction time fixed at 5 h (central run), the surface regions which exhibited the best results in terms of n_{COOH} were 500 mg $\leqslant w_{NaNO_2} \leqslant$ 970 mg and 11 mL $\leqslant V_{H_3PO_4} \leqslant$ 19 mL for both materials (Cel and SB). This observation agrees with the experimental data, where the largest

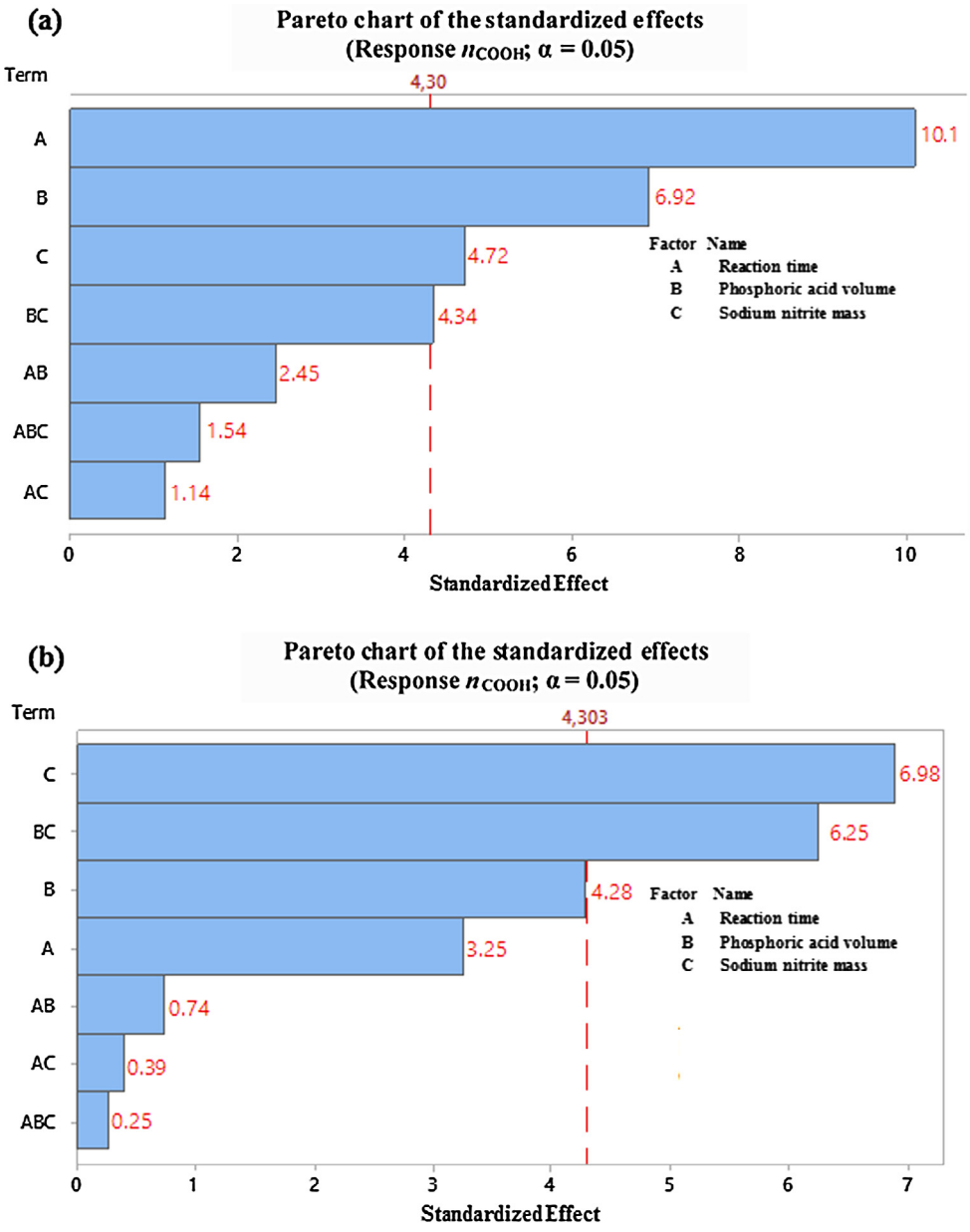

Fig. 2. Pareto's charts for the optimization of the oxidation reaction of (a) Cel and (b) SB.

Table 2
Regression coefficients in terms of uncoded variable levels for the oxidation of cellulose and sugarcane bagasse.

Regression coefficients	Cellulose		Sugarcane bagasse	
	Coefficients in terms of uncoded variables	*p*-value	Coefficients in terms of uncoded variables	*p*-value
a_0	−1.900	0.000	1.630	0.000
a_1	1.080	0.119	0.328	0.001
a_2	0.427	0.009	0.0759	0.001
a_3	0.00531	0.003	0.00415	0.003
a_4	−0.0925	0.188	−0.0309	0.004
a_5	−0.0220	0.106	−0.00634	0.000
a_6	−0.000005	0.014	−0.000005	0.008
a_7	0.0103	0.777	0.00286	0.314
a_8	−0.000048	0.881	0.000030	0.809
a_9	0.000174	0.047	0.000193	0.060

Table 3
Analysis of variance (ANOVA) for the oxidation of cellulose and sugarcane bagasse.

Factor	DF	SS	MS	F-value	*p*-value
		Oxidized cellulose (Cox)			
t	1	3.2325	3.2325	45.55	0.001
V	1	2.7430	2.7430	38.65	0.001
w	1	1.6418	1.6418	23.13	0.003
t^2	1	3.2806	1.4781	20.83	0.004
V^2	1	1.4781	3.2806	15.42	0.000
w^2	1	1.0944	1.0944	46.22	0.008
$t \times V$	1	0.3802	0.0045	1.21	0.314
$t \times w$	1	0.0045	0.3802	0.06	0.809
$V \times w$	1	0.0857	0.0857	5.36	0.060
Lack of fit	4	0.3670	0.0917	3.12	0.257
Pure error	2	0.0589	0.0294		
Total SS	16	36.2903			
		Oxidized sugarcane bagasse (SBox)			
t	1	0.2468	0.2468	3.30	0.119
V	1	1.1056	1.0194	14.79	0.009
w	1	1.7058	1.1056	22.81	0.003
t^2	1	0.1650	0.1650	2.21	0.188
V^2	1	0.2711	0.2711	3.63	0.014
w^2	1	0.8762	0.8762	11.72	0.106
$t \times V$	1	0.0066	0.0066	0.09	0.777
$t \times w$	1	0.0018	0.0018	0.02	0.881
$V \times w$	1	0.4651	0.4651	6.22	0.047
Lack of fit	4	0.4248	0.1062	8.92	0.103
Pure error	2	0.0238	0.0119		
Total SS	16	37.5722			

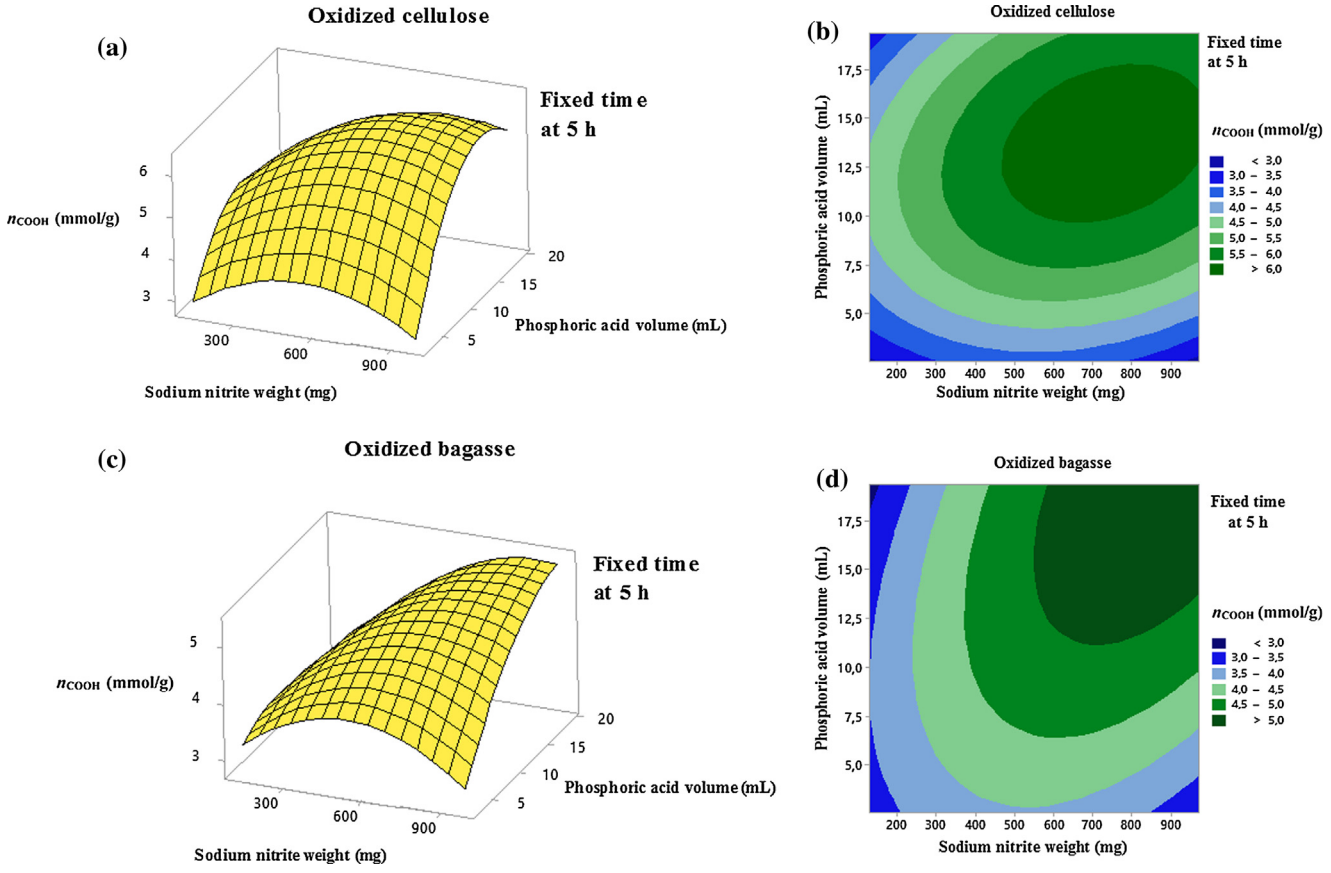

Fig. 3. Response surfaces (left) and contour lines (right) for the dependent variable n_{COOH} for the oxidation of (a) and (b) cellulose and (c) and (d) sugarcane bagasse.

n_{COOH} values were found using a reaction time of 5 h with values of w_{NaNO_2} and $V_{H_3PO_4}$ within the range previously described.

3.2. Characterization of oxidized cellulose and sugarcane bagasse

The oxidation of the hydroxyl groups of Cel and SB to carboxylic acid groups using a mixture of $NaNO_2$ and H_3PO_4 to produce oxidized cellulose (Cox) and sugarcane bagasse (SBox) was carried out using the synthetic route presented in Fig. 4.

The oxidation reaction allowed the conversion of the hydroxyl groups of Cel and SB into carboxylic acid groups. The carboxylic group is a weak acid that can dissociate in aqueous solution to produce a carboxylate group, which contains a negative charge that is stabilized by resonance. The negative charges of carboxylate groups are able to interact with cationic dyes, promoting an electrostatic interaction and removing the dye molecules from aqueous solutions by adsorption [9,38].

After Cel oxidation, a weight gain of 7.7% was noticed due to the conversion of the primary hydroxyl groups to carboxylic acid groups, increasing the molar mass of AGU [28]. In the case of SB oxidation, a weight loss of 18.4% was observed. This weight loss can be explained by the acidic conditions and the presence of oxidant species, which are able to degrade biopolymers such as hemicelluloses and lignin, increasing their solubility in aqueous solution [37]. The n_{COOH} for Cox and SBox was determined by acid-base back-titration and found to be 4.8 mmol/g and 4.5 mmol/g, respectively. For Cox, this result corresponds to a modification of 85% of the primary hydroxyl groups of the starting cellulose. Such a value represents a high degree of conversion. The values of n_{COOH} reported in the literature for oxidized cellulose are in the range from 0.2 to 4.0 mmol/g [27,39,40]. Compared to the literature data, Cox and SBox showed a higher degree of oxidation and consequently a higher value of n_{COOH}, thereby demonstrating the importance of design of experiments in the optimization of the proposed reactions. For SBox, although a weight loss was noticed, a high value of n_{COOH} was obtained, demonstrating that the method optimized in this study can be successfully applied to an agricultural waste, producing a more valuable material.

The characterization of Cox and SBox was accomplished by FTIR spectroscopy. FTIR spectra of cellulose (Cel) and oxidized cellulose (Cox) as well as raw sugarcane bagasse (SB) and oxidized sugarcane bagasse (SBox) are shown in Fig. 5a and b, respectively. The major changes that can be seen in the FTIR spectrum of Cox in comparison to Cel and SBox in comparison to SB are the presence of a strong band at 1728 cm^{-1}, which is attributed to C=O stretching in carboxylic acid groups and the intensification of the band at 1736 cm^{-1} in SBox. These bands confirm the conversion of hydroxyl groups of Cel and SB to carboxylic acid groups, producing Cox and SBox [41].

In addition, the SB FTIR spectrum in Fig. 5b shows bands at 1519 cm^{-1} and 1600 cm^{-1}, which can be attributed to the aromatic rings of syringyl and guaiacyl units, respectively. The great decrease in the intensity of these bands in the spectrum of SBox probably indicates that most of the lignin was removed from SB by oxidation [42].

Cox was also characterized by solid-state ^{13}C NMR spectroscopy. The SS ^{13}C NMR spectrum of Cox shown in Fig. 6 suggests that non-oxidized cellulose is still present in the oxidized product due to the signals at 62 ppm and 93 ppm, which correspond to C-6 and C-4 of the starting cellulose, respectively, although in minor amounts. This result confirms that 85% of the primary hydroxyl groups of the starting cellulose were modified. The main product is Cox with signals at 104 ppm and 83 ppm corresponding to the anomeric carbon atoms at C-1 and C-4, respectively [42]. The signal at 73 ppm can be attributed to the superposition of signals from C-2, C-3 and C-5. The main evidence of Cox formation is the presence of a strong signal at 172 ppm, which can be attributed to the carbonyl carbon of the carboxylic acid group. A weak signal at 228 ppm is also present, suggesting that ketone formation at C-3 or C-2 may also have occurred. Ketone formation should not affect negatively the behavior of the material in dye adsorption, as ketone is a polar group with unshared electron pairs. Due to the presence of a mixture of oxidized polymers, SBox was not analyzed by SS ^{13}C NMR spectroscopy.

Analysis of the plots of equilibrium pH as a function of weight-to-volume percent for Cox and SBox (figures not shown) indicate the net surface charge of the adsorbent materials Cox and SBox. The pH of zero charge (pH_{PZC}) for Cox and SBox was 2.70 and 2.72, respectively. This means that at pH values greater that 2.7 both adsorbent materials are negatively charged, thereby favoring the adsorption of the cationic dyes CV and AO [15].

Thermogravimetric (TGA) and derivative thermogravimetric curves (DTG) for Cel, Cox, SB and SBox are shown in Supplementary Fig. 1. As can be seen in Supplementary Fig. 1a–d and Table 4, the initial small weight loss, which occurred at temperatures between 44 and 55 °C, representing approximately 6–11% of the total weight loss, was attributed to the vaporization of bound water in the samples. The TGA curves for Cel (Supplementary Fig. 1a) and Cox (Supplementary Fig. 1b) exhibited one main decomposition event. The major difference in the TGA curves for Cox and Cel is a drastic decrease of the maximum decomposition temperature, T_m (DTG peak) in Cox. $T_{m,2}$ for Cel was 369 °C and $T_{m,2}$ for Cox was 243 °C, showing a lower thermal stability for Cox. This result also confirms that the chemical conversion of Cel to Cox was successful. The TGA curve of SB (Supplementary Fig. 1c) exhibited two

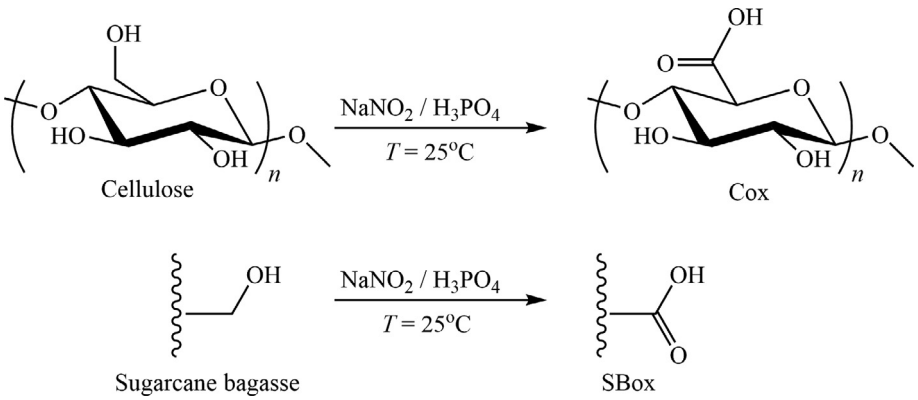

Fig. 4. Synthetic route used to prepare oxidized cellulose (Cox) and sugarcane bagasse (SBox).

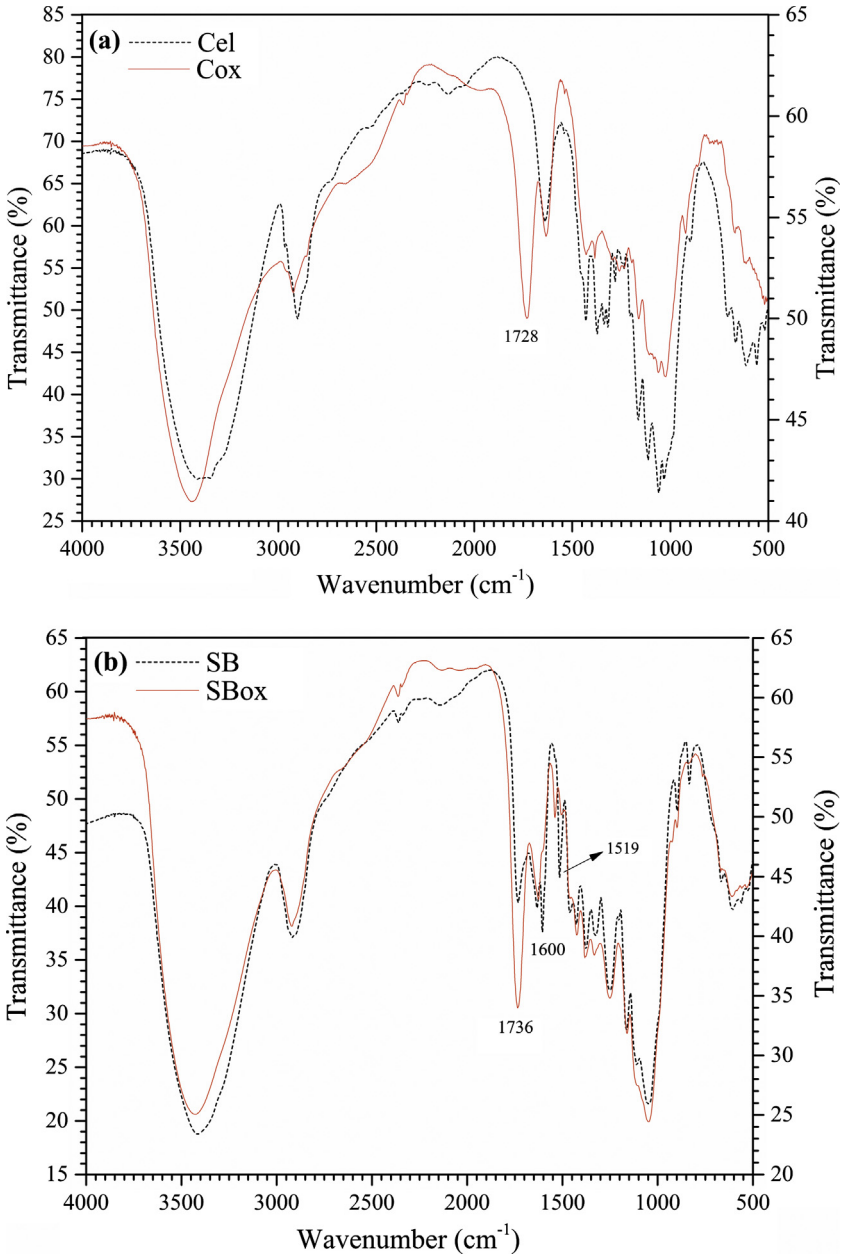

Fig. 5. FTIR spectra of (a) cellulose (Cel) and oxidized cellulose (Cox) and (b) raw sugarcane bagasse (SB) and oxidized sugarcane bagasse (SBox).

main decomposition events. The DTG peaks at $T_{m,2}$ = 317 °C and $T_{m,3}$ = 379 °C for SB are attributed to the decomposition of hemicellulose and cellulose, which break down faster than lignin, yielding volatile compounds [43]. The TGA curve for SBox (Supplementary Fig. 1d) also exhibited two main decomposition events. As was observed for Cox in comparison to Cel, SBox compared to SB showed a drastic decrease in the maximum decomposition temperature, $T_{m,2}$ (from 317 °C to 252 °C) and $T_{m,3}$ (from 379 °C to 309 °C), demonstrating the lower thermal stability of SBox. The fact that SBox presents more decomposition events than Cox shows that oxidized lignin or hemicelluloses are still present in the final product and oxidation did not totally eliminate the lignin and hemicellulose content of the SB.

Fig. 7a–d shows SEM images of Cel and Cox at 60 and 500×, respectively. In Fig. 7a and b, it is noted that raw cellulose used in the oxidation reaction presents preserved fibers even after milling process. However, some fibers exhibited partial degradation of primary cell wall (Fig. 7b). Fig. 7c shows that Cox does not present a fiber shape as a result of the degradation of fibers during oxidation process. Cox particles present a great heterogeneity of shapes and sizes. Fig. 7d also shows that oxidation process of Cel led to the formation of particles with a heterogeneous surface, including the presence of roles of different sizes [44].

Fig. 7e–h shows SEM images of SB and SBox at 60 and 500×, respectively. Fig. 7e shows that raw SB presents particles of different sizes and shapes as a results of the heterogeneity of cell elements from fiber and pith fractions. In Fig. 7f, it is noted that both fiber and pith fractions were partially degraded during the milling process. In Fig. 7g and h, it is noted that the fibers were exposed due to the oxidation of lignin and hemicellulose fractions, and the solubilization of these macromolecules led to the appearance of roles and cracks in the surface of the fiber and pith fractions [17].

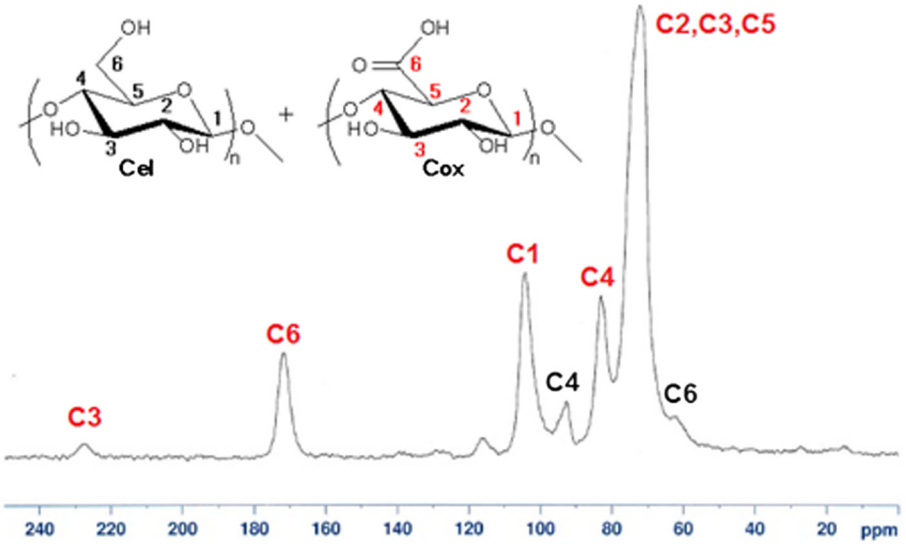

Fig. 6. Solid-state ^{13}C NMR spectra of oxidized cellulose (Cox).

Table 4
Thermogravimetric data for the thermal decomposition of cellulose (Cel), oxidized cellulose (Cox), sugarcane bagasse (SB) and oxidized sugarcane bagasse (SBox).

Parameters[a]	Cel	Cox	SB	SBox
T_{onset} (°C)	347	198	271	208
$T_{D,1}$ (°C)	20	20	14	15
$T_{m,1}$ (°C)	44	50	49	54
ΔW_1 (%)	6.3	10.9	10.1	10.5
$T_{D,2}$ (°C)	259	152	175	122
$T_{m,2}$ (°C)	369	243	317	252
ΔW_2 (%)	94.9	67.9	31.0	34.4
$T_{D,3}$ (°C)	–	–	333	293
$T_{m,3}$ (°C)	–		379	309
ΔW_3 (%)	–	–	45.7	31.0

[a] T_{onset}: onset temperature, T_D : initial decomposition temperature, T_m : maximum decomposition temperature (DTG peak), ΔW_i : weight loss in the decomposition event.

3.3. Adsorption studies

3.3.1. Effect of the solution pH on dye uptake by Cox and SBox

The effect of the solution pH on the adsorption is a very important parameter affecting the removal of charged adsorbates such as CV and AO. Since Cox and SBox are adsorbent materials that contain carboxylic acid groups, which are ionizable, the adsorption of CV and AO is pH-dependent. The adsorption capacity (q_e) for CV and AO as a function of the solution pH for Cox and SBox is shown in Fig. 8a and b.

As can be seen in Fig. 8a, the adsorption capacity of CV on Cox increased as the solution pH was increased and a plateau was reached at pH 6 for CV whilst the adsorption capacity of AO continued to increase as the solution pH was increased. Fig. 8b shows that the adsorption of both dyes by SBox increased as the solution pH was increased and plateaus were reached at pH 6 for both dyes. The pH_{PZC} of Cox and SBox are 2.70 and 2.72, respectively, indicating that at pH values higher than ~2.7 both adsorbent materials have negative surface charges and are able to adsorb both dyes from aqueous solution. As can be seen in Fig. 8a and b, the adsorption capacity of Cox and SBox for CV and AO is high even at low pH, thereby confirming that both adsorbent materials can efficiently adsorb CV and AO even at low pH values, which is in good agreement with the values of pH_{PZC}. A similar tendency was noticed by Gusmao et al. [9] for the adsorption of the cationic dyes methylene blue (MB) and crystal violet (CV) by succinylated sugarcane bagasse (SCB 2), another adsorbent material containing carboxylic acid groups on its surface.

As a plateau was not reached for the adsorption of AO by Cox and there is a possibility of the structural modification of AO [45] at pH values higher than 8.0, a pH value of 8.0 was considered as the optimum pH value for adsorption of AO, in order to prevent any degradation of the dye. For comparison purposes, the subsequent studies of adsorption of CV by Cox and SBox as a function of contact time and initial dye concentration were performed at a pH value of 8.0.

3.3.2. Adsorption kinetics

Predicting the rate at which the adsorption of a pollutant takes place in a particular system is probably the most important factor in the design of an adsorption system [46]. Experiments examining the adsorption of CV and AO by Cox and SBox were performed to determine the adsorption rate constants and equilibrium times. In order to investigate the mechanism of dye adsorption on Cox and SBox, three kinetic models were evaluated: pseudo-first-order (PFO), pseudo-second-order (PSO) and Elovich.

The PFO kinetic model of Lagergren [47] assumes that the adsorption rate is a function of the adsorption capacity as shown in Eq. (11):

$$q_t = q_e[1 - \exp(-k_1 t)] \tag{11}$$

where q_e (mg/g) is the adsorption capacity at equilibrium, q_t (mg/g) is the adsorption capacity at a time t (min) and k_1 (min^{-1}) is the PFO rate constant [48–50].

If the adsorption mechanism occurs by chemisorption, it can be represented by the PSO kinetic model [49,50]. The mathematical expression of this model is shown in Eq. (12):

$$q_t = \frac{k_2 q_e^2 t}{1 + k_2 q_e t} \tag{12}$$

where k_2 (g/mg min) is the PSO rate constant.

A general interpretation of the Elovich equation (EE)[51] involves the variation of the chemisorption energy with the coverage of the adsorbent surface. The equation of this model can be described by Eq. (13):

$$q_t = \frac{1}{\beta}\ln(\alpha\beta) + \frac{1}{\beta}\ln t \tag{13}$$

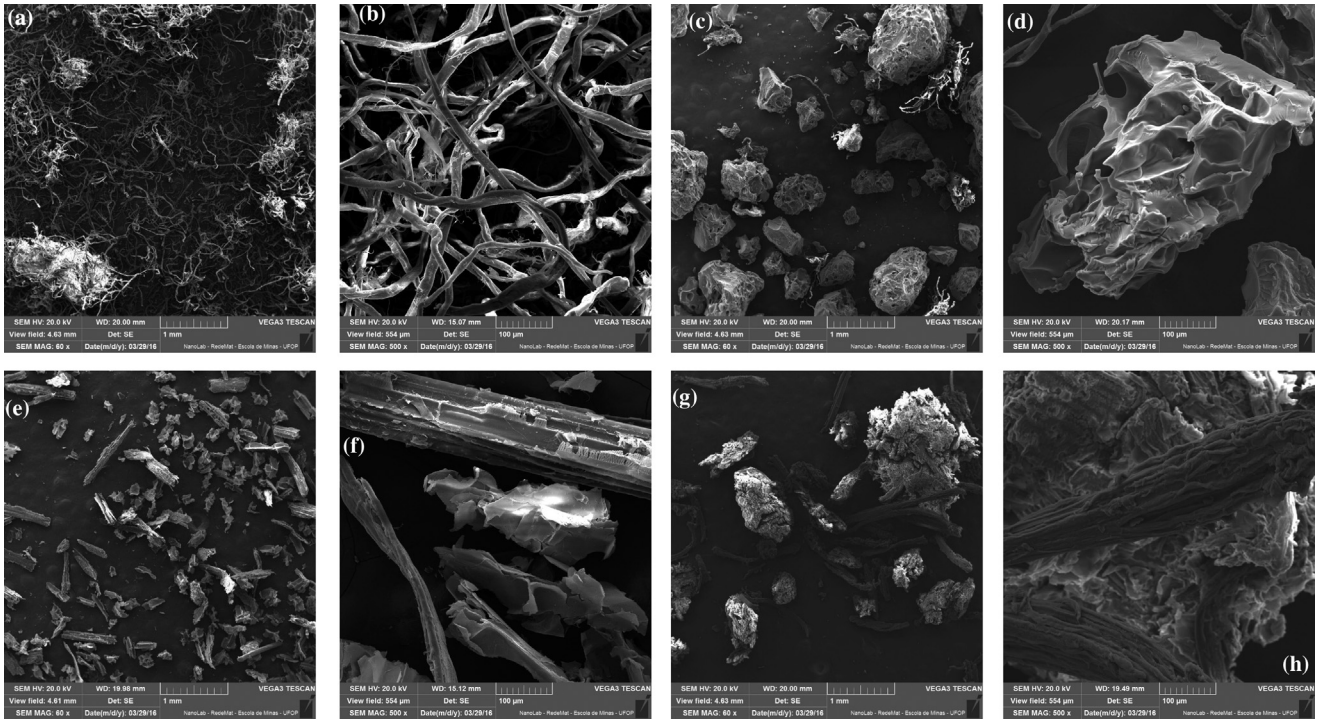

Fig. 7. SEM images of raw cellulose (Cel) (a and b), oxidized cellulose (Cox) (c and d), raw sugarcane bagasse (SB) (e and f) and oxidized sugarcane bagasse (SBox) (g and h) at 60 and 500× magnification, respectively.

where α (mg/g min) is the initial adsorption rate and β (g/mg) is the desorption constant [52,53].

The experimental kinetic data were modeled by nonlinear regression (NLR) analysis using the PFO, PSO and EE models using Microcal OriginPro® software (2015). The software was set to use the Levenberg–Marquardt algorithm and the weight method named "statistical". To define which model best describes the adsorption process, the determination coefficient (R^2) and the reduced chi-square (χ^2_{red}) were evaluated [54].

Fig. 9a and b shows the curves of the NRL analysis as a result of the modeling the experimental data using the PFO, PSO and EE models. Table 5 shows the parameters estimated by the kinetic models. As can be seen in Fig. 9a, the adsorption equilibrium time (t_e) for the adsorption of CV and AO on Cox was attained after 12 h (720 min) for CV and 9 h (540 min) for AO. The t_e for adsorption of CV and AO on SBox was attained after 9 h (540 min) for CV and 5 h (300 min) for AO. Comparing the values of the determination coefficients, R^2, and the reduced chi-square, χ^2_{red} shown in Table 5, it can be observed that the adsorption of CV by Cox was better fitted by the Elovich model, and therefore, chemisorption may be the step controlling the rate of adsorption for this system. As suggested by the EE model, there may be a variation in the adsorption energy with increasing surface coverage of the adsorbent for this system. Another plausible explanation suggested by the EE model is the heterogeneity of the nature of the active surface sites, displaying different activation energies for chemisorption [53]. Concerning the adsorption of AO by Cox, the best fit was found using the PFO model. The adsorption of CV and AO by SBox was better described by the PSO model. Therefore, it is assumed that for these systems the rate limiting step of adsorption may be governed by chemisorption involving the sharing or exchange of electrons between the adsorbent and adsorbate [50].

3.3.3. Adsorption isotherms

An adsorption isotherm can describe how an adsorbate interacts with an adsorbent and is important in optimizing the use of an adsorbent in real adsorption processes. Furthermore, it is crucial to have a good estimate of the adsorption capacity of the adsorbent for application purposes [2]. Various isotherm models are available in the literature, and four of them were chosen to evaluate the equilibrium results i.e. the Langmuir, Freundlich, Redlich-Peterson (R-P) and Konda models.

The Langmuir [55] isotherm theory assumes a monolayer coverage of adsorbate on a homogeneous surface of the adsorbent. Graphically, the Langmuir isotherm is characterized by a plateau. Therefore, at equilibrium, the saturation point is reached when adsorption cannot occur. In addition, adsorption occurs at specific adsorption sites on the homogeneous surface of the adsorbent. Once a dye molecule occupies a site, there can be no adsorption there [56]. The Langmuir isotherm is presented by Eq. (14):

$$q_e = \frac{Q_{max} b C_e}{1 + b C_e} \tag{14}$$

where q_e (mg/g) is the equilibrium adsorption capacity, Q_{max} (mg/g) is the maximum amount of the dye per unit weight of Cox or SBox, C_e (mg/L) is the concentration of adsorbate in the liquid phase at equilibrium and b (L/mg) is the Langmuir constant related to the affinity of the adsorbate at the binding sites.

The changes in free energy ($\Delta_{ads}G^\circ$) of adsorption can be calculated using Eq. (15) (Liu [57]):

$$\Delta_{ads}G^\circ = -RT \ln K_a \tag{15}$$

where K_a is the thermodynamic equilibrium constant (dimensionless), T (K) is the absolute temperature and R (8.314 J/K mol) is the ideal gas constant.

The thermodynamic equilibrium constant can be calculated from the Langmuir constant, b, using the approach suggested by Liu [57] and presented by Eq. (16):

$$K_a = \left[\frac{b}{\gamma_e}(1\ \text{mol/L})\right] \tag{16}$$

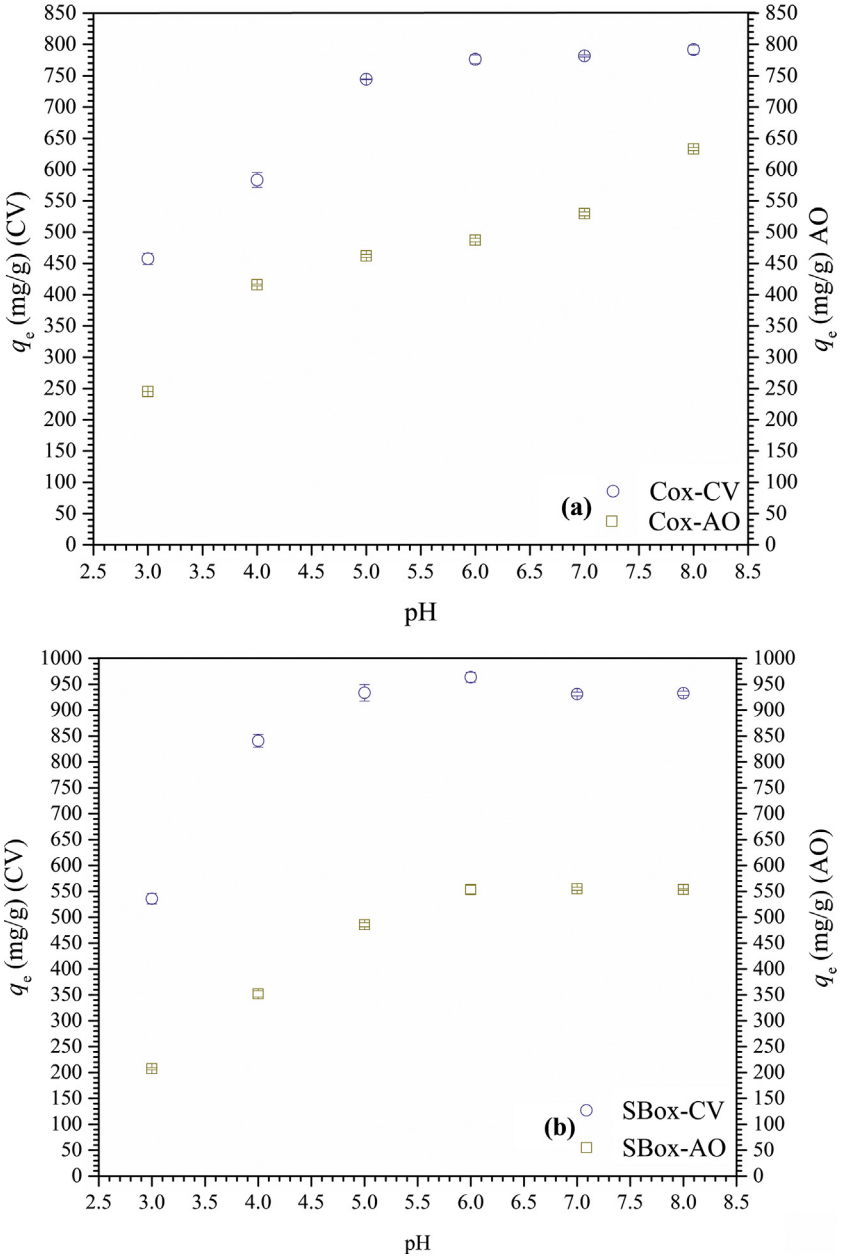

Fig. 8. Effect of initial pH on the adsorption of CV and AO on (a) Cox and (b) SBox (200 mg/L CV or AO, 25 °C, 150 rpm, 0.2 g/L Cox or SBox).

where γ_e is the activity coefficient at equilibrium (dimensionless). In the case of neutral or weakly charged adsorbates, such as organic dyes, the Langmuir constant, b (L/mol), can be reasonably used to calculate $\Delta_{ads}G°$ because $\gamma_e \sim 1$ [57].

The Freundlich [58] isotherm model is an empirical equation, which is applicable to adsorption on heterogeneous surfaces and is not restricted to the formation of a monolayer. It is assumed that an increase in adsorbate concentration also increases the amount adsorbed on the surface of the adsorbent. From this perspective, the adsorbed amount is the sum of the adsorbate adsorption at all binding sites (each with its binding energy), where the sites with higher binding energy are occupied first. There is an exponential decrease in the adsorption power until the process is complete [56]. The model is presented by Eq. (17):

$$q_e = K_F C_e^{1/n} \tag{17}$$

where K_F [(mg/g)(L/mg)$^{1/n}$] and n are the Freundlich constants. The parameter n is usually greater than unity and it is related to the adsorption intensity.

The Redlich and Peterson [59](R-P) isotherm model can be applied to homogeneous and heterogeneous systems. This model is a combination of the characteristics of the Langmuir and Freundlich models and provides a more realistic representation of the adsorption system at higher concentrations [60]. The R-P model is presented by Eq. (18):

$$q_e = \frac{K_R C_e}{1 + a_R C_e^{\beta}} \tag{18}$$

where K_R (L/g) e a_R (L/mg) are the R-P constants and β is the R-P parameter, which must be between 0 and 1. When β approaches zero, the equation is reduced to the Henry's equation and when β

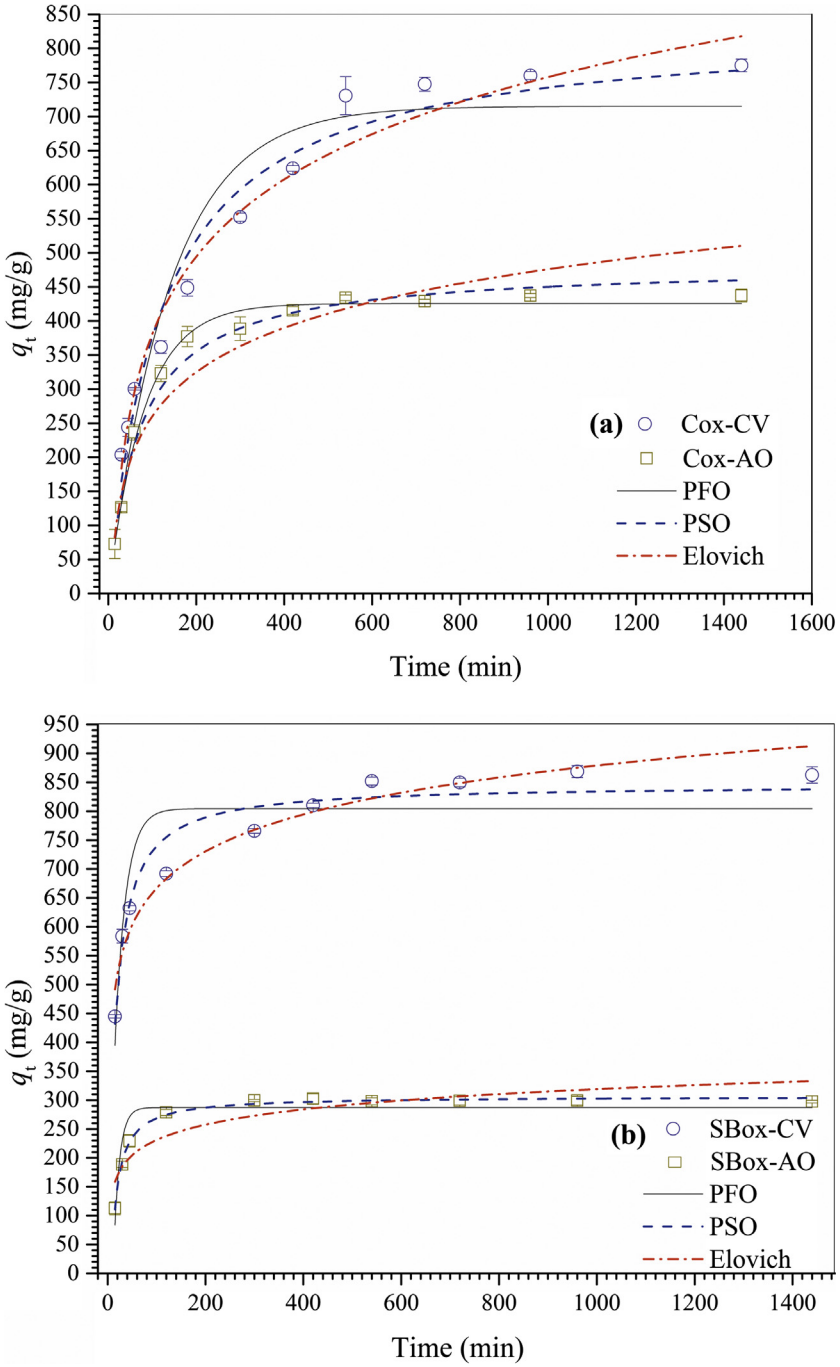

Fig. 9. Effect of contact time on adsorption of (a) CV and AO on Cox and (b) CV and AO on SBox. (200 mg/L CV or AO, pH = 8, 25 °C, 150 rpm and 0.2 g/L Cox or SBox).

tends to 1 the system is reduced to the Langmuir model and the adsorption behavior approaches a homogeneous system [60,61].

Assuming possible interactions between the adsorbed molecules and the presence of active sites with steric hindrance and energy heterogeneity, Konda et al. [62] have proposed a nonlinear mathematical model to describe multilayer adsorption from the sum of Langmuir type isotherms. This model assumes the existence of different and specific mechanisms at each stage of adsorption demonstrated by the profile of the curve. It introduces a parameter related to a critical concentration above which a new adsorption mechanism becomes effective. The equation proposed by Konda et al. [62] is shown in Eq. (19):

$$q_e = \frac{a_1 K_1 C}{1 + K_1 C} + \frac{a_2 K_2 [(C - b_2) + |C - b_2|]}{2 + K_2 [(C - b_2) + |C - b_2|]} \quad (19)$$

where q_e (mg/g) is the adsorption capacity at equilibrium, a_i (mg/g) and K_i (L/mg) are the adsorption capacity and adsorption constant related to different layers, respectively, and b_i (mg/L) is the critical limit concentration of the adsorption mechanism on a given layer. The maximum adsorption capacity, Q_{max} (mg/g), can be obtained by the sum of the adsorption capacities in different layers.

The isotherms for the adsorption of CV and AO on Cox and SBox are presented in Fig. 10a and b. It is well established that the profile of the isotherms is largely determined by the adsorption

Table 5
Modeled kinetic parameters for the adsorption of CV and AO by SBox and Cox (200 mg/L CV or AO, pH = 8, 25 °C, 150 rpm and 0.2 g/L Cox or SBox).

Parameters	Cox-CV	Cox-AO	SBox-CV	SBox-AO
$q_{e,exp}$ (mg/g)	775.0	437.4	868.8	504.6
$q_{e,exp}$ (mmol/g)	1.900	1.439	2.129	1.237
Pseudo-first-order kinetic model				
k_1 (min^{-1})	7.14×10^{-3}	1.23×10^{-2}	0.044	0.085
$q_{e,est}$ (mg/g)	715.2	425.7	804.5	496.5
$q_{e,est}$ (mmol/g)	1.753	1.401	2.017	1.217
R^2	0.916	0.995	0.836	0.850
χ^2_{red}	9.228	0.434	5.704	0.698
Pseudo-second-order kinetic model				
k_2 (g/mg min)	9.89×10^{-6}	2.89×10^{-5}	8.22×10^{-5}	3.68×10^{-4}
$q_{e,est}$ (mg/g)	832.6	482.5	845.9	509.6
$q_{e,est}$ (mmol/g)	2.041	1.588	2.073	1.677
R^2	0.966	0.988	0.955	0.995
χ^2_{red}	3.681	1.183	1.555	0.020
Elovich model				
α (mg/g min)	16.73	14.93	1267	1.08×10^{7}
β (g/mg)	6.10×10^{-3}	1.06×10^{-2}	1.08×10^{-2}	3.83×10^{-2}
R^2	0.976	0.954	0.953	0.799
χ^2_{red}	2.576	4.731	1.620	0.938

mechanism [63]. Giles et al. [64] proposed a classification of isotherm profiles using the characteristics that may be attributed to adsorption processes. According to their classification, the profiles of the curves corresponding to the adsorption of CV and AO on SBox and CV on Cox are in the L group and subgroup 2, and the curve corresponding to the adsorption of AO on Cox is in the L group and subgroup 4. Thus, the initial curvature (type L) in these adsorption systems indicates that there is increased difficulty in finding available active sites on the surfaces of the adsorbent materials with increasing coverage. It also implies that the dye molecules may not be oriented vertically or there may not be a strong competition between the adsorbent and solvent for the dye. Adsorption systems classified in subgroup 2 are characterized by monolayer adsorption with a plateau indicating the saturation of the adsorption surface sites, and adsorption systems classified in subgroup 4 are characterized by adsorption with the formation of a second layer. According to Liu [65], adsorption processes that deviate from Langmuir isotherm behavior can be described by models that describe multilayer adsorption. Also, according to Liu [61], due to heterogeneity in the energy of the active sites or interactions of adsorbate molecules to be adsorbed with adsorbate molecules already fixed in an active site, the adsorption process can result in an apparently sequential adsorption or multilayer adsorption (cooperative adsorption). Thus, even if the physical orientation of the adsorbate on the adsorbent surface is a monolayer it is possible that the adsorption system can be described by a model that allows multilayer adsorption.

The selection of the best isotherm model describing the adsorption systems was based on the evaluation of R^2 values together with χ^2_{red} values. Table 6 shows the estimated isotherm parameters obtained by modeling the experimental isotherm data with the Langmuir, Freundlich, Redlich-Peterson and Konda models. Comparing the values of R^2 and χ^2_{red}, it can be seen that more than one model shows a satisfactory fit to the experimental data. A joint analysis of these models can provide relevant information about the systems studied.

The adsorption of CV on SBox was best fitted by the Langmuir and Redlich-Peterson models, with the same R^2 value. The most suitable model was determined by the evaluation of χ^2_{red}, which takes into account the degrees of freedom of the models evaluated. This analysis showed that the Langmuir model best describes this adsorption system. The Q_{max} for CV adsorption on SBox according to the Langmuir model was found to be 1018.2 mg/g. The Q_{max} value of the Langmuir model is closer to the experimental adsorption capacity, $Q_{max,exp}$, thereby confirming the good fit of the model to the experimental data. In addition, Q_{max} for CV adsorption on SB was found to be 72.6 mg/g, thereby showing that oxidation reaction greatly improved the adsorption capacity of SBox in comparison to SB. The value of change in free energy of adsorption ($\Delta_{ads}G^o$) and b shows an energetically favorable adsorption process with the highest affinity of the adsorbate for adsorbent surface sites among all the studied systems. The β parameter of the R-P model is close to 1, thereby showing that this adsorption system approaches the Langmuir model, indicating a more homogeneous adsorption system [61]. According to Mall et al. [66], when the R-P equation reduces to the Langmuir equation, the values of a_R and K_R/a_R are equivalent to the values of b and Q_{max} of the Langmuir model, respectively. The good correlation between the parameters of these different models is evidenced by the proximity of their values in this study, highlighting again the good agreement between the experimental data and the data estimated by the model. Therefore, the analysis of the isotherm models indicates that the adsorption of CV on SBox may occur predominantly in a monolayer with a more homogeneous distribution of dye molecules along the surface sites of the adsorbent.

The adsorption of AO on Cox and SBox was better fitted by the Konda multilayer isotherm model. The Freundlich model showed a good fit for both materials whilst the Redlich-Peterson model showed a good fit only for SBox. The Q_{max} values for AO adsorption on Cox and SBox estimated by the Konda model were found to be 1223.3 and 682.8 mg/g, respectively. Moreover, Q_{max} for AO adsorption on Cel and SB were found to be 13.0 and 27.8 mg/g, which shows that oxidized materials (Cox and SBox) exhibited a much higher adsorption capacity compared to non-oxidized materials. Although the profile of the curve for the adsorption of AO on SBox was classified as L2 [64], the model that best fitted the experimental data was that describing the formation of multilayers. The evaluation of the profile of the experimental curve (L4) and the good agreement of the Konda and Freundlich models with the experimental data imply that the adsorption of AO on Cox may be influenced by interactions between adsorbate molecules (cooperative adsorption) and may not be restricted to the formation of a monolayer. For both adsorption systems, the parameters a_1 and a_2 obtained by the Konda model indicate the first and second adsorption capacity of the double layer adsorption. Comparing these parameters, it can be seen that a higher adsorption capacity was achieved through the mechanism involved in the formation of

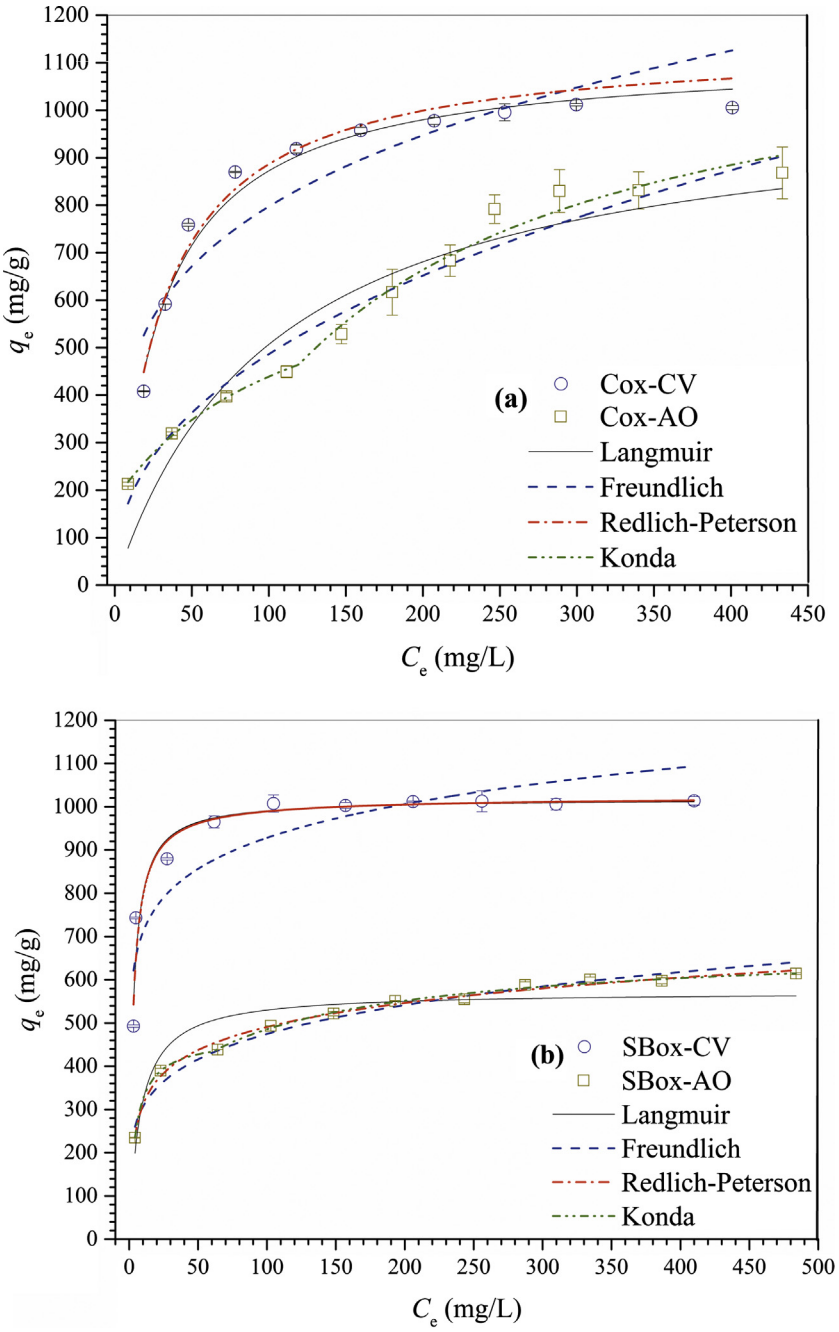

Fig. 10. Isotherms for adsorption of (a) CV and AO on Cox and (b) CV and AO on SBox (pH = 8, 25 °C, 150 rpm and 0.2 g/L Cox or SBox).

the first layer of adsorbate on the adsorbent for SBox and a higher adsorption capacity in the formation of the second layer for Cox. The value of b_2 gives the concentration limit where a change in the adsorption mechanism occurs. The concentration must be greater than 60.92 and 119.42 mg /L for AO adsorption on SBox and Cox, respectively. When this concentration is exceeded, there is a possibility of the formation of a new layer of dye molecules or active sites with different energy content. The β parameter of the R-P model for AO adsorption on SBox is further from unity and consequently shows more a heterogeneous character for this adsorption system in comparison with CV adsorption on SBox. The value of $1/n$ of the Freundlich model for both adsorption systems is between 0 and 1, indicating that the adsorption process is energetically favorable [56,67,68]. Thus, analysis of these results leads to the conclusion that the adsorption of AO by Cox and SBox may not be restricted to the formation of a monolayer, and interactions between the dye molecules may be influencing the adsorption behavior, with a non-uniform distribution of adsorption heats and affinities of AO dye for the adsorption sites.

As seen in Table 6, considering the values of R^2 and χ^2_{red}, the adsorption of CV on Cox was best described by the Langmuir and R-P models, with the best fit for the Langmuir model. The Q_{max} for CV adsorption on Cox estimated by the Langmuir model was found to be 1117.8 mg/g. The proximity of the value of Q_{max} estimated by the Langmuir model in comparison to the experimental adsorption capacity, $Q_{max,exp}$, indicates the good correlation between the experimental data and those estimated by the model. In contrast, Q_{max} for CV adsorption on Cel was found to be 8.6 mg/g. The value of change in free energy of adsorption ($\Delta_{ads}G^o$) and b shows an energetically favorable adsorption. The β parameter of the R-P model is

Table 6
Isotherm model parameters for the adsorption of CV and AO on Cox and SBox (pH = 8, 25 °C, 150 rpm and 0.2 g/L Cox or SBox).

Isotherm models	Parameters	Cox-CV	Cox-AO	SBox-CV	SBox-AO
Experimental data	$Q_{max,exp}$ (mg/g)	1004.4	843.1	1011.0	604.1
	$Q_{max,exp}$ (mmol/g)	2.696	3.141	2.712	2.250
Langmuir	$Q_{max,exp}$ (mg/g)	1117.8	1036.6	1018.2	571.8
	$Q_{max,exp}$ (mmol/g)	3.000	3.863	2.732	2.131
	b (L/mg)	0.036	9.57×10^{-3}	0.358	0.126
	b (L/mol)	13,224	2569	133,372	33,809
	R^2	0.978	0.876	0.956	0.912
	χ^2_{red}	1.576	15.450	2.385	3.903
	$\Delta G°$ (kJ/mol)	−23.51	−19.45	−29.24	−25.84
Freundlich	K_F [(mg/g)/(L/mg)$^{1/n}$]	253.8	69.59	543.3	197.6
	n	4.02	2.37	8.60	5.26
	$1/n$	0.248	0.422	0.116	0.190
	R^2	0.859	0.966	0.827	0.979
	χ^2_{red}	11.427	4.129	9.393	0.888
Redlich-Peterson	K_R (L/g)	39.4	–	372.6	205.1
	a_R (L/mg)	0.034	–	0.372	0.771
	K_R/a_R (mg/g)	1145.0	–	1001.5	266.1
	K_R/a_R (mmol/g)	3.075	–	2.689	0.991
	β	1.000	–	0.996	0.861
	R^2	0.976	–	0.956	0.995
	χ^2_{red}	2.181	–	2.719	0.240
Konda	a_1 (mg/g)	–	565.5	–	422.2
	a_2 (mg/g)	–	657.8	–	206.6
	$Q_{max,exp}$ (mg/g)	–	1223.3	–	682.8
	$Q_{max,exp}$ (mmol/g)	–	4.558	–	2.544
	K_1 (L/mg)	–	8.56×10^{-3}	–	0.193
	K_2 (L/mg)	–	4.54×10^{-3}	–	5.6×10^{-3}
	b_2 (mg/L)	–	119.42	–	60.92
	R^2	–	0.992	–	0.998
	χ^2_{red}	–	1.422	–	0.102

equal to 1, indicating that the R-P isotherm model approaches the Langmuir model. Thus, as can be seen in Table 6, the value of a_R and K_R/a_R can be related to the values of b and Q_{max} estimated by the Langmuir model, respectively [66]. Therefore, the behavior of this adsorption system can be better described by the Langmuir model, indicating a monolayer formation with a homogeneous distribution of adsorption energy on the surface of the adsorbent [61,69].

3.4. Desorption and reuse of the adsorbents Cox and SBox

Desorption studies using Cox and SBox loaded with the CV and AO dyes were performed at pH 1.3 and 2 (HCl 0.05 mol/L and 0.01 mol/L), respectively. The high concentration of hydronium ions (H_3O^+) at these pH values enables the removal of the model dyes from the surface of the adsorbents by an ion exchange mechanism, where H_3O^+ ions protonate the carboxylate groups present on the surface of Cox and SBox, releasing the dye molecules to aqueous solution. Eqs. (20) and (21) present the adsorption and desorption mechanisms by which dye molecules of CV or AO are adsorbed by the solid support (SS) (Cox or SBox) and desorbed from the SS to acidic solution, respectively. The desorption efficiencies (E_{des}) for SBox-CV, Cox-CV, SBox-AO and Cox-AO were 50.47%, 51.82%, 50.03% and 50.19%, respectively.

$$\text{SS-COOH} + \text{dye}^+ \overset{H_2O}{\rightleftharpoons} \text{SS-COOdye} + H_3O^+ \quad (20)$$

$$\text{SS- COOdye} + H_3O^+ \rightleftharpoons \text{SS- COOH} + \text{dye}^+ + H_2O \quad (21)$$

Studies reported in the literature have demonstrated diverse desorption efficiencies of CV and AO from different solid supports (adsorbents). Ferreira et al. [17] achieved a removal of 57.9% of CV with an aqueous HCl solution (0.01 mol/L) from carboxylated sugarcane bagasse. Ahmad [70] achieved desorption efficiencies of 67.5% and 88% for CV adsorbed from powder of pine bark using aqueous NaCl (1 mol/L) and CH_3COOH (1 mol/L) solutions, respectively. Kumar and Ahmad [71], using aqueous CH_3COOH (0.01 mol/L) and CH_3COOH (1 mol/L) solutions, obtained about 35% and 50% efficiency for CV desorption from ginger rhizome treated with $H_2SO_4/ZnCl_2$. Mall et al., [66] obtained only 2% desorption efficiency using an aqueous 0.1 mol/L HCl solution and 4% using 0.1 mol/L HNO_3 solution for AO desorption from fertilizer plant waste carbon. Inbaraj et al. [72] achieved 98% AO desorption from the biopolymer poly(γ-glutamic acid) at pH 1.

The incomplete removal of CV and AO from Cox and SBox means that there is a strong interaction between these dyes and the active surface sites on the adsorbents. It also indicates that the nature of the dye adsorption on the solid supports is not purely an electrostatic interaction involving an ion exchange mechanism [17,66,71–74].

Re-adsorption studies were performed to evaluate the possibility of reuse of the adsorbents. Although the desorption of the dyes was not complete, Cox and SBox still exhibited good re-adsorption efficiencies compared to their initial adsorption capacities. The re-adsorption efficiencies (*RE*) for CV on SBox and Cox were 65.64% and 69.66%, while the *RE* for AO on SBox and Cox were 80.91% and 77.01%, respectively. It is clear that the materials presented in this study, even when partially loaded, show superior results to various adsorbents described in the literature [66,71,72]. These results suggest that even with partial loss of their adsorption capacities, SBox and Cox are interesting materials from the point of view of their reuse.

3.5. Comparison with literature data for CV and AO adsorption on different adsorbent materials

The data presented in Table 7 show the maximum adsorption capacities for the more efficient adsorbents found in the literature

Table 7
Comparison of different adsorbent materials reported in the literature for removal of CV and AO from aqueous solutions.

Adsorbent	Dye	T (°C)	t_e (min)	Q_{max} (mg/g)	Reference
Cox	AO	25	540	1223.2	This study
SBox	AO	25	300	682.8	This study
Nanohydrogel	AO	25	1440	337.8	[75]
Fertilizer plant waste carbon	AO	25	300	246.2	[66]
Chromium doped zinc oxide nanoparticles	AO	25	4 (sonication)	211.6	[76]
ZnS-Cu nanoparticles loaded on activated carbon	AO	25	2.2 (sonication)	94.2	[77]
Bagasse fly ash	AO	30	120	31.7	[78]
Activated carbon	AO	30	120	12.5	[78]
Cox	CV	25	720	1117.7	This study
SBox	CV	25	540	1018.2	This study
Acid-treated montmorillonite	CV	30	180	400.0	[79]
Raw Montmorillonite	CV	30	180	370.4	[79]
Spent tea leaves	CV	50	60	285.7	[80]
Treated ginger waste	CV	50	150	277.7	[71]
Fertilizer plant waste carbon	CV	25	300	240.26	[66]
Nanoparticles based on modified rice husk	CV	30	720	97.7	[81]
Succinylated sugarcane bagasse	CV	25	1200	1273.2	[9]
Sugarcane bagasse modified with EDTA dianhydride	CV	25	900	327.8	[82]
Carboxylate-functionalized cellulose nanocrystals	CV	30	240	243.9	[19]
Sugarcane bagasse modified with Meldrum's acid	CV	25	720	692.1	[17]
Modified cellulose with glycidyl methacrylate	CV	50	150	218.8	[83]

used for the removal of crystal violet (CV) and auramine-O (AO). The value of AO adsorption capacity found in this study for Cox and SBox is considerably higher than those found in previous studies reported in the literature. In addition, for CV adsorption, the values of Q_{max} obtained in the present study are higher than those reported in most previous studies. Only one adsorbent with a slightly better adsorption capacity in comparison with those reported in the present study has been reported, produced by the succinylation of sugarcane bagasse [9].

4. Conclusions

Oxidized cellulose (Cox) and sugarcane bagasse (SBox) were synthesized using optimized experimental conditions obtained through a design of experiments (DOE) and a response surface methodology (RSM). Cox and SBox were characterized by FTIR, TGA, PZC and solid-state ^{13}C NMR. Cox and SBox presented 4.8 mmol/g and 4.5 mmol/g of carboxylic acid groups, respectively. The Cox and SBox adsorbents were very effective in the removal of the model cationic dyes crystal violet (CV) and auramine-O (AO) from aqueous solutions. The adsorption of CV and AO on Cox was described by pseudo-first-order kinetic and Elovich models, respectively, while the adsorption of CV and AO on SBox was described by a pseudo-second-order kinetic model. The adsorption isotherms were evaluated by four adsorption models and the experimental data fitted well to the Langmuir (CV) and Konda (AO) models. Maximum adsorption capacities (Q_{max}) for CV and AO on Cox were found to be 1117.8 and 1223.3 mg/g, respectively, while the Q_{max} for CV and AO on SBox were found to be 1018.2 and 682.8 mg/g.

Acknowledgments

The authors are grateful to Universidade Federal de Ouro Preto (UFOP), Fundação de Amparo à Pesquisa do Estado de Minas Gerais – Brazil (FAPEMIG grant number CEX APQ-01945/13, CEX APQ-01764/14 and a doctoral scholarship awarded to L.R. Martins) and Conselho Nacional de Desenvolvimento Científico – Brazil (CNPq grant number 448346/2014-1) for funding this research. The authors are also grateful to Laboratório de microscopia eletrônica, microanálises e caracterização de materiais (NanoLab/FINEP) – RedeMat Escola de Minas, UFOP and B.S. Ney P. Sampaio for SEM–EDX analyses.

Appendix A. Supplementary material

Supplementary data associated with this article can be found, in the online version, at http://dx.doi.org/10.1016/j.jcis.2017.01.085.

References

[1] A.B. dos Santos, F.J. Cervantes, J.B. van Lier, Review paper on current technologies for decolourisation of textile wastewaters: perspectives for anaerobic biotechnology, Bioresour. Technol. 98 (12) (2007) 2369–2385.
[2] M.T. Yagub, T.K. Sen, S. Afroze, H.M. Ang, Dye and its removal from aqueous solution by adsorption: a review, Adv. Colloid Interface Sci. 209 (2014) 172–184.
[3] E. Forgacs, T. Cserháti, G. Oros, Removal of synthetic dyes from wastewaters: a review, Environ. Int. 30 (7) (2004) 953–971.
[4] M.C. Costa, S. Mota, R.F. Nascimento, A.B. Dos Santos, Anthraquinone-2,6-disulfonate (AQDS) as a catalyst to enhance the reductive decolourisation of the azo dyes Reactive Red 2 and Congo Red under anaerobic conditions, Bioresour. Technol. 101 (1) (2010) 105–110.
[5] M. Deravanesiyan, M. Beheshti, A. Malekpour, Alumina nanoparticles immobilization onto the NaX zeolite and the removal of Cr (III) and Co (II) ions from aqueous solutions, J. Ind. Eng. Chem. 21 (2015) 580–586.
[6] I. Laaz, M.-J. Stébé, A. Benhamou, D. Zoubir, J.-L. Blin, Influence of porosity and surface modification on the adsorption of both cationic and anionic dyes, Colloids Surf. A. 490 (2016) 30–40.
[7] L. Hou, F. Jiang, S. Wang, Synthesis and characteristics of macroporous epoxy resin-triethylenetetramine polymer modified by sodium chloroacetate for copper chelation in aqueous solution, Annali Chimica 97 (10) (2007) 995–1003.
[8] L.V.A. Gurgel, O.K. Junior, R.P.D.F. Gil, L.F. Gil, Adsorption of Cu(II), Cd(II), and Pb (II) from aqueous single metal solutions by cellulose and mercerized cellulose chemically modified with succinic anhydride, Bioresour. Technol. 99 (8) (2008) 3077–3083.
[9] K.A.G. Gusmao, L.V.A. Gurgel, T.M.S. Melo, L.F. Gil, Application of succinylated sugarcane bagasse as adsorbent to remove methylene blue and gentian violet from aqueous solutions – kinetic and equilibrium studies, Dyes Pigm. 92 (3) (2012) 967–974.
[10] CONAB, Companhia Nacional de Abastecimento (CONAB). Acompanhamento da safra brasileira de cana-de-açúcar, segundo levantamento da safra 2015/2016, in: CONAB (Ed.) Brasília, Brazil, 2015, pp. 16–20.
[11] O. Karnitz, L.V.A. Gurgel, J.C.P. de Melo, V.R. Botaro, T.M.S. Melo, R.P.D.F. Gil, L.F. Gil, Adsorption of heavy metal ion from aqueous single metal solution by chemically modified sugarcane bagasse, Bioresour. Technol. 98 (6) (2007) 1291–1297.
[12] D. Klemm, B. Heublein, H.P. Fink, A. Bohn, Cellulose: fascinating biopolymer and sustainable raw material, Angewandte Chemie-Int. Ed. 44 (22) (2005) 3358–3393.
[13] S. Hokkanen, A. Bhatnagar, M. Sillanpää, A review on modification methods to cellulose-based adsorbents to improve adsorption capacity, Water Res. 91 (2016) 156–173.
[14] S. Afroze, T. Sen, M. Ang, Agricultural solid wastes in aqueous phase dye adsorption: a review, in: C. Foster (Ed.), Agricultural Wastes: Characteristics, Types and Management, Nova Publishers, USA, 2015, pp. 169–213.

[15] S.N.d.C. Ramos, A.L.P. Xavier, F.S. Teodoro, L.F. Gil, L.V.A. Gurgel, Removal of cobalt(II), copper(II), and nickel(II) ions from aqueous solutions using phthalate-functionalized sugarcane bagasse: mono- and multicomponent adsorption in batch mode, Ind. Crop. Prod. 79 (2016) 116–130.
[16] J.-X. Yu, J. Zhu, L.-Y. Feng, R.-A. Chi, Simultaneous removal of cationic and anionic dyes by the mixed sorbent of magnetic and non-magnetic modified sugarcane bagasse, J. Colloid Interf. Sci. 451 (2015) 153–160.
[17] B.C.S. Ferreira, F.S. Teodoro, A.B. Mageste, L.F. Gil, R.P. de Freitas, L.V.A. Gurgel, Application of a new carboxylate-functionalized sugarcane bagasse for adsorptive removal of crystal violet from aqueous solution: kinetic, equilibrium and thermodynamic studies, Ind. Crop. Prod. 65C (2015) 521–534.
[18] S. Kumari, D. Mankotia, G.S. Chauhan, Crosslinked cellulose dialdehyde for Congo red removal from its aqueous solutions, J. Environ. Chem. Eng. 4 (1) (2016) 1126–1136.
[19] H. Qiao, Y. Zhou, F. Yu, E. Wang, Y. Min, Q. Huang, L. Pang, T. Ma, Effective removal of cationic dyes using carboxylate-functionalized cellulose nanocrystals, Chemosphere 141 (2015) 297–303.
[20] F. Gellerstedt, P. Gatenholm, Surface properties of lignocellulosic fibers bearing carboxylic groups, Cellulose 6 (2) (1999) 103–121.
[21] R.R. Navarro, K. Sumi, M. Matsumura, Improved metal affinity of chelating adsorbents through graft polymerization, Water Res. 33 (9) (1999) 2037–2044.
[22] T. Tashiro, Y. Shimura, Removal of mercuric ions by systems based on cellulose derivatives, J. Appl. Polym. Sci. 27 (2) (1982) 747–756.
[23] A.J. Varma, V.B. Chavan, A study of crystallinity changes in oxidised celluloses, Polym. Degrad. Stabil. 49 (2) (1995) 245–250.
[24] S. Coseri, G. Biliuta, B.C. Simionescu, K. Stana-Kleinschek, V. Ribitsch, V. Harabagiu, Oxidized cellulose—survey of the most recent achievements, Carbohydr. Polym. 93 (1) (2013) 207–215.
[25] A.E.J. de Nooy, A.C. Besemer, H. van Bekkum, Highly selective nitroxyl radical-mediated oxidation of primary alcohol groups in water-soluble glucans, Carbohyd. Res. 269 (1) (1995) 89–98.
[26] V. Kumar, T. Yang, $HNO_3/H_3PO4–NaNO_2$ mediated oxidation of cellulose — preparation and characterization of bioabsorbable oxidized celluloses in high yields and with different levels of oxidation, Carbohydr. Polym. 48 (4) (2002) 403–412.
[27] A.E.J. de Nooy, M. Pagliaro, H. van Bekkum, A.C. Besemer, Autocatalytic oxidation of primary hydroxyl functions in glucans with nitrogen oxides, Carbohyd. Res. 304 (2) (1997) 117–123.
[28] R. Andersson, J. Hoffman, N. Nahar, E. Scholander, An n.m.r. study of the products of oxidation of cellulose and (1 → 4)-β-d-xylan with sodium nitrite in orthophosphoric acid, Carbohyd. Res. 206 (2) (1990) 340–346.
[29] N. Isobe, X. Chen, U.-J. Kim, S. Kimura, M. Wada, T. Saito, A. Isogai, TEMPO-oxidized cellulose hydrogel as a high-capacity and reusable heavy metal ion adsorbent, J. Hazard. Mater. 260 (2013) 195–201.
[30] S.N.C. Ramos, A.L.P. Xavier, F.S. Teodoro, M.M.C. Elias, F.J. Gonçalves, L.F. Gil, R. P. Freitas, L.V.A. Gurgel, Modeling mono-and multi-component adsorption of cobalt (II), copper (II), and nickel (II) metal ions from aqueous solution onto a new carboxylated sugarcane bagasse. Part I: Batch adsorption study, Ind. Crop. Prod. 74 (2015) 357–371.
[31] D.C. Montgomery, Design and Analysis of Experiments, fifth ed., John Wiley & Sons, New York, 2000.
[32] J.S. Noh, J.A. Schwarz, Effect of HNO_3 treatment on the surface-acidity of activated carbons, Carbon 28 (5) (1990) 675–682.
[33] F.S. Teodoro, S.N.d.C. Ramos, M.M.C. Elias, A.B. Mageste, G.M.D. Ferreira, L.H.M. da Silva, L.F. Gil, L.V.A. Gurgel, Synthesis and application of a new carboxylated cellulose derivative. Part I: Removal of Co^{2+}, Cu^{2+} and Ni^{2+} from monocomponent spiked aqueous solution, J. Colloid Interf. Sci. 483 (2016) 185–200.
[34] G.M. Laisha, V.I. Sharkov, The kinetics of oxidation of celluloses by nitrogen tetroxide as a characteristic of their supermolecular structure, Polym. Sci. U.S. S.R. 16 (8) (1974) 1971–1978.
[35] T.J. Painter, A. Cesàro, F. Delben, S. Paoletti, New glucuronoglucans obtained by oxidation of amylose at position 6, Carbohyd. Res. 140 (1) (1985) 61–68.
[36] S.M. de Vasconcelos, A.M.P. Santos, G.J.M. Rocha, A.M. Souto-Maior, Diluted phosphoric acid pretreatment for production of fermentable sugars in a sugarcane-based biorefinery, Bioresour. Technol. 135 (2013) 46–52.
[37] C.A. Rezende, M.A. de Lima, P. Maziero, E.R. deAzevedo, W. Garcia, I. Polikarpov, Chemical and morphological characterization of sugarcane bagasse submitted to a delignification process for enhanced enzymatic digestibility, Biotechnol. Biofuels 4 (1) (2011) 1–19.
[38] M.A. Hubbe, K.R. Beck, W.G. Neal, Y.C. Sharma, Cellulosic substrates for removal of pollutants from aqueous systems: a review. 2. Dyes, Bioresources 7 (2) (2012) 2592–2687.
[39] Y. Xu, X. Liu, X. Liu, J. Tan, H. Zhu, Influence of $HNO_3/H_3PO_4–NaNO_2$ mediated oxidation on the structure and properties of cellulose fibers, Carbohydr. Polym. 111 (13) (2014) 955–963.
[40] M. Hirota, N. Tamura, T. Saito, A. Isogai, Oxidation of regenerated cellulose with $NaClO_2$ catalyzed by TEMPO and NaClO under acid-neutral conditions, Carbohydr. Polym. 78 (2) (2009) 330–335.
[41] E. Pehlivan, H.T. Tran, W.K.I. Ouédraogo, C. Schmidt, D. Zachmann, M. Bahadir, Sugarcane bagasse treated with hydrous ferric oxide as a potential adsorbent for the removal of As(V) from aqueous solutions, Food Chem. 138 (1) (2013) 133–138.
[42] L.B. Brenelli, F. Mandelli, A.Z. Mercadante, G.J.d.M. Rocha, S.A. Rocco, A.F. Craievich, A.R. Gonçalves, D.d.C. Centeno, M. de Oliveira Neto, F.M. Squina, Acidification treatment of lignin from sugarcane bagasse results in fractions of reduced polydispersity and high free-radical scavenging capacity, Ind. Crop. Prod. 83 (2016) 94–103.
[43] G. Varhegyi, M.J. Antal, T. Szekely, P. Szabo, Kinetics of the thermal decomposition of cellulose, hemicellulose, and sugarcane bagasse, Energ Fuel 3 (3) (1989) 329–335.
[44] V.B. Chavan, B.D. Sarwade, A.J. Varma, Morphology of cellulose and oxidised cellulose in powder form, Carbohydr. Polym. 50 (1) (2002) 41–45.
[45] R.J. Goldacre, J.N. Phillips, The ionization of basic triphenylmethane dyes, J. Chem. Soc. (1949) 1724–1732.
[46] Y.-S. Ho, Review of second-order models for adsorption systems, J. Hazard. Mater. 136 (3) (2006) 681–689.
[47] S.Y. Lagergren, Zur theorie der sogenannten adsorption gelöster stoffe, kungliga svenska vetenskapsakademiens, Handlingar 24 (4) (1898) 1–39.
[48] Y.S. Ho, G. McKay, Kinetic models for the sorption of dye from aqueous solution by wood, Process Saf. Environ. Prot. 76 (2) (1998) 183–191.
[49] Y.S. Ho, G. McKay, Sorption of dye from aqueous solution by peat, Chem. Eng. J. 70 (2) (1998) 115–124.
[50] Y.S. Ho, G. McKay, Pseudo-second order model for sorption processes, Process Biochem. 34 (5) (1999) 451–465.
[51] S.Z. Roginsky, Y.B. Zeldovich, Acta Physicochimica U.S.S.R. 1 (1934) 554.
[52] M. Özacar, İ.A. Şengil, A kinetic study of metal complex dye sorption onto pine sawdust, Process Biochem. 40 (2) (2005) 565–572.
[53] C.W. Cheung, J.F. Porter, G. McKay, Sorption kinetic analysis for the removal of cadmium ions from effluents using bone char, Water Res. 35 (3) (2001) 605–612.
[54] F.T.R.D. Almeida, B.C.S. Ferreira, A.L.D.S.L. Moreira, R.P.D. Freitas, L.F. Gil, L.V.A. Gurgel, Application of a new bifunctionalized chitosan derivative with zwitterionic characteristics for the adsorption of Cu^{2+}, Co^{2+}, Ni^{2+}, and oxyanions of Cr^{6+} from aqueous solutions: kinetic and equilibrium aspects, J. Colloid Interf. Sci. 466 (2016) 297–309.
[55] I. Langmuir, The adsorption of gases on plane surfaces of glass, mica and platinum, J. Am. Chem. Soc. 40 (9) (1918) 1361–1403.
[56] K.Y. Foo, B.H. Hameed, Insights into the modeling of adsorption isotherm systems, Chem. Eng. J. 156 (1) (2010) 2–10.
[57] Y. Liu, Is the free energy change of adsorption correctly calculated?, J Chem. Eng. Data 54 (7) (2009) 1981–1985.
[58] H.M. Freundlich, Over the adsorption in solution, Z Phys. Chem.-Stoch Ve 57 (4) (1906) 385–470.
[59] O. Redlich, D.L. Peterson, A useful adsorption isotherm, J. Phys. Chem. 63 (6) (1959). 1024-1024.
[60] B. Stephen Inbaraj, C.P. Chiu, G.H. Ho, J. Yang, B.H. Chen, Removal of cationic dyes from aqueous solution using an anionic poly-γ-glutamic acid-based adsorbent, J. Hazard. Mater. 137 (1) (2006) 226–234.
[61] J.C.Y. Ng, W.H. Cheung, G. McKay, Equilibrium studies of the sorption of Cu(II) ions onto chitosan, J. Colloid Interf. Sci. 255 (1) (2002) 64–74.
[62] L.N. Konda, I. Czinkota, G. Füleky, G. Morovján, Modeling of single-step and multistep adsorption isotherms of organic pesticides on soil, J. Agr. Food Chem. 50 (25) (2002) 7326–7331.
[63] C.H. Giles, D. Smith, A. Huitson, A general treatment and classification of the solute adsorption isotherm. I. Theoretical, J. Colloid Interf. Sci. 47 (3) (1974) 755–765.
[64] C.H. Giles, T.H. MacEwan, S.N. Nakhwa, D. Smith, Studies in adsorption. Part XI. A system of classification of solution adsorption isotherms, and its use in diagnosis of adsorption mechanisms and in measurement of specific surface areas of solids, J. Chem. Soc. (1960) 3973–3993.
[65] S. Liu, Cooperative adsorption on solid surfaces, J. Colloid Interf. Sci. 450 (2015) 224–238.
[66] I.D. Mall, V.C. Srivastava, G.V.A. Kumar, I.M. Mishra, Characterization and utilization of mesoporous fertilizer plant waste carbon for adsorptive removal of dyes from aqueous solution, Colloids Surf., A 278 (1–3) (2006) 175–187.
[67] E. Alver, A.Ü. Metin, Anionic dye removal from aqueous solutions using modified zeolite: adsorption kinetics and isotherm studies, Chem. Eng. J. 200–202 (2012) 59–67.
[68] S.J. Allen, Q. Gan, R. Matthews, P.A. Johnson, Comparison of optimised isotherm models for basic dye adsorption by kudzu, Bioresour. Technol. 88 (2) (2003) 143–152.
[69] S. Álvarez-Torrellas, A. Rodríguez, G. Ovejero, J. García, Comparative adsorption performance of ibuprofen and tetracycline from aqueous solution by carbonaceous materials, Chem. Eng. J. 283 (2016) 936–947.
[70] R. Ahmad, Studies on adsorption of crystal violet dye from aqueous solution onto coniferous pinus bark powder (CPBP), J. Hazard. Mater. 171 (1–3) (2009) 767–773.
[71] R. Kumar, R. Ahmad, Biosorption of hazardous crystal violet dye from aqueous solution onto treated ginger waste (TGW), Desalination 265 (1–3) (2011) 112–118.
[72] B.S. Inbaraj, J.T. Chien, G.H. Ho, J. Yang, B.H. Chen, Equilibrium and kinetic studies on sorption of basic dyes by a natural biopolymer poly(γ-glutamic acid), Biochem. Eng. J. 31 (3) (2006) 204–215.
[73] V.M. Esquerdo, T.R.S. Cadaval Jr., G.L. Dotto, L.A.A. Pinto, Chitosan scaffold as an alternative adsorbent for the removal of hazardous food dyes from aqueous solutions, J. Colloid Interf. Sci. 424 (2014) 7–15.
[74] G.L. Dotto, J.M.N. Santos, I.L. Rodrigues, R. Rosa, F.A. Pavan, E.C. Lima, Adsorption of Methylene Blue by ultrasonic surface modified chitin, J. Colloid Interf. Sci. 446 (2015) 133–140.
[75] V.P. Mahida, M.P. Patel, Removal of some most hazardous cationic dyes using novel poly (NIPAAm/AA/N-allylisatin) nanohydrogel, Arabian J. Chem. 9 (3) (2016) 430–442.

[76] M. Jamshidi, M. Ghaedi, K. Dashtian, S. Hajati, A.A. Bazrafshan, Sonochemical assisted hydrothermal synthesis of ZnO: Cr nanoparticles loaded activated carbon for simultaneous ultrasound-assisted adsorption of ternary toxic organic dye: Derivative spectrophotometric, optimization, kinetic and isotherm study, Ultrason. Sonochem. 32 (2016) 119–131.
[77] A. Asfaram, M. Ghaedi, S. Hajati, M. Rezaeinejad, A. Goudarzi, M.K. Purkait, Rapid removal of Auramine-O and Methylene blue by ZnS: Cu nanoparticles loaded on activated carbon: a response surface methodology approach, J. Taiwan Inst. Chem. Eng. 53 (2015) 80–91.
[78] I.D. Mall, V.C. Srivastava, N.K. Agarwal, Adsorptive removal of Auramine-O: kinetic and equilibrium study, J. Hazard. Mater. 143 (1–2) (2007) 386–395.
[79] G.K. Sarma, S. Sen Gupta, K.G. Bhattacharyya, Adsorption of Crystal violet on raw and acid-treated montmorillonite, K10, in aqueous suspension, J. Environ. Manage. 171 (2016) 1–10.
[80] S.K. Bajpai, A. Jain, Equilibrium and thermodynamic studies for adsorption of crystal violet onto spent tea leaves (STL), Water 4 (2012) 52–71.
[81] A. Masoumi, K. Hemmati, M. Ghaemy, Low-cost nanoparticles sorbent from modified rice husk and a copolymer for efficient removal of Pb(II) and crystal violet from water, Chemosphere 146 (2016) 253–262.
[82] K.A.G. Gusmão, L.V.A. Gurgel, T.M.S. Melo, L.F. Gil, Adsorption studies of methylene blue and gentian violet on sugarcane bagasse modified with EDTA dianhydride (EDTAD) in aqueous solutions: Kinetic and equilibrium aspects, J. Environ. Manage. 118 (2013) 135–143.
[83] Y. Zhou, M. Zhang, X. Wang, Q. Huang, Y. Min, T. Ma, J. Niu, Removal of Crystal Violet by a novel cellulose-based adsorbent: comparison with native cellulose, Ind. Eng. Chem. Res. 53 (13) (2014) 5498–5506.